Chapter 8 in the book:
P.A. Kralchevsky and K. Nagayama, "Particles at Fluid Interfaces and Membranes"
(Attachment of Colloid Particles and Proteins to Interfaces and Formation of Two-Dimensional Arrays)
Elsevier, Amsterdam, 2001; pp. 351-395.

CHAPTER 8

LATERAL CAPILLARY FORCES BETWEEN FLOATING PARTICLES

This chapter contains theoretical and experimental results about the lateral capillary interaction between two floating particles, and between a floating particle and a vertical wall. The origin of this "flotation" force is the overlap of the interfacial deformations created by the separate floating particles. The difference between the "flotation" and "immersion" forces is manifested through the distinct physical origin of the respective "capillary charge" Q, which results in a different dependence of Q on the interfacial tension σ and particle radius R. In some aspect these two kinds of capillary interactions resemble the electrostatic and gravitational forces, which obey the same power law, but differ in the physical meaning and magnitude of the force constants (charges, masses). Theoretical expressions for calculating the capillary charges and interaction energy of two floating particles are obtained. Numerical results for the dependence of the interaction energy on the interparticle distance, particle radius, density and contact angle are presented and discussed. In all cases the dependence of force vs. distance is a monotonic attraction or repulsion depending on whether the particles are similar or dissimilar.

A single particle floating in a vicinity of a vertical wall experiences the action of a "capillary image force". The latter can be formally considered as an interaction between the particle and its mirror image. This force can be attractive or repulsive depending on whether the contact angle or contact line is fixed at the wall. The presence of an inclined meniscus in a neighborhood of the wall may lead to a non-monotonic dependence of the interaction energy on the particle-wall separation. This dependence is derived by means of both energy and force approaches. A convenient asymptotic formula for the capillary force is obtained, which compares very well with the output of the more accurate theory. The derived expressions are in a very good agreement with experimental data for the equilibrium position of floating particles. The obtained theoretical results have been applied to determine the surface drag coefficient of floating particles and the surface shear viscosity of surfactant adsorption monolayers.

8.1. INTERACTION BETWEEN TWO FLOATING PARTICLES

8.1.1. FLOTATION FORCE: THEORETICAL EXPRESSION IN SUPERPOSITION APPROXIMATION

Similarly to the derivation of the asymptotic formula for the *immersion* force (see Section 7.1.3 above), one can apply the superposition approximation to derive an expression for the *flotation* force, which is valid for not-too-small distances between the particles. Following Nicolson [1] let us consider a floating spherical particle of mass m_k, which creates an interfacial deformation, see Fig. 8.1. Equation (7.8) for $k = 1, 2$, which describes the meniscus profile $\zeta_k(r)$ around each of the two particles in isolation, holds again. The geometrical configuration and the meaning of the parameters is illustrated in Fig. 8.1 for $k = 1$.

The force due to gravity (weight + buoyancy), $F_{g(k)}$, which is exerted on the k-th particle ($k = 1, 2$) is counterbalanced by the vertically resolved surface tension force, acting per unit length of the three-phase contact line:

$$F_{g(k)} = 2\pi\sigma r_k \sin\psi_k = 2\pi\sigma Q_k \qquad (k = 1,2) \qquad (8.1)$$

see Fig. 8.1 and Eq. (2.2). Here $F_{g(k)} = m_k g - F_b$ with F_b being the buoyancy (Archimedes) force.; expression for F_b for floating particles can be found in Ref. [2]; see Eq. (8.8) below.

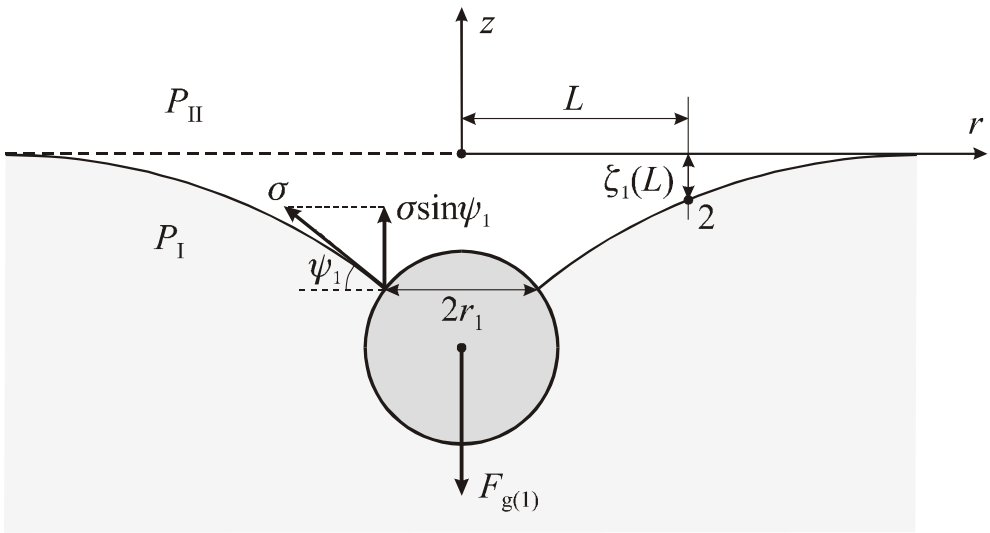

Fig. 8.1. A heavy spherical particle creates a concave meniscus on an otherwise horizontal fluid interface of tension σ; $F_{g(1)}$ is the net force due to gravity (a combination of particle weight and buoyancy); ψ_1 is the meniscus slope at the particle contact line of radius r_1.

Let us consider particle 2 situated at a horizontal distance L from particle 1. After Nicolson [1] we assume that due to the existence of a meniscus created by particle 1, the mass-center of particle 2 is situated at a distance $\zeta_1(L)$ below the horizontal plane $z = 0$, see point 2 in Fig. 8.1. The work carried out by the gravitational force to bring particle 2 from level $z = 0$ (infinite interparticle separation) down to level $z = -\zeta_1(L)$ is [1,3]

$$\Delta W_g = - F_{g(2)}\zeta_1(L) = - 2\pi\sigma Q_1 Q_2 \mathrm{K}_0(qL) \tag{8.2}$$

where at the last step Eqs. (7.8) and (8.1) have been used. Having in mind that

$$F = -\frac{d\Delta W_g}{dL}; \qquad \frac{dK_0(x)}{dx} = -K_1(x) \tag{8.3}$$

one obtains that (at not-too-small distances) the flotation force, likewise the immersion force, obeys the asymptotic law [1,3]

$$F = -2\pi\sigma Q_1 Q_2 q \mathrm{K}_1(qL), \qquad r_k << L. \tag{8.4}$$

The above derivation of Eq. (8.4) makes use of several approximations – see the discussion after Eq. (7.13) above. Expressions, which are more accurate than Eq. (8.4) can be found in Section 8.1.4.

As already noticed, the equation $F = -2\pi\sigma Q_1 Q_2 q \mathrm{K}_1(qL)$ expresses the derivative of *wetting* energy in the case of *immersion* force, and the derivative of *gravitational* energy in the case of *flotation* force. The fact that the results are formally identical stems from the usage of the same expression for the meniscus shape, viz. Eq. (7.8). Indeed, the meniscus shape (the solution of Laplace equation) "feels" the interacting bodies only through the boundary condition that the meniscus slope is ψ_k at $r = r_k$, irrespective of the physical cause of the interfacial deformation (the capillary rise in Fig. 7.3. or the particle weight in Fig. 8.1). As a result, we have $F \propto \mathrm{K}_1(qL)$ for both immersion and flotation lateral capillary forces; however, the coefficient of proportionality, Q_1Q_2 depends on the type of the capillary force, as demonstrated below.

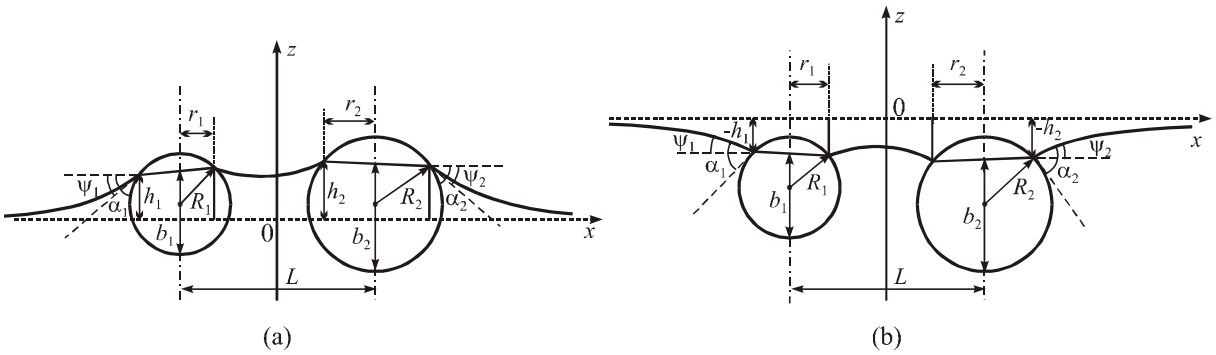

Fig. 8.2. Sketch of two floating particles of radii R_1 and R_2 separated at a center-to-center distance L. (a) Two light particles. (b) Two heavy particles. r_1 and r_2 are the radii of the contact lines, α_1 and α_2 are three-phase contact angles, ψ_1 and ψ_2 are meniscus slope angles; h_1 and h_2 are the elevations of the contact lines with respect to the level $z = 0$ of the non-disturbed horizontal interface far from the floating particles.

8.1.2. "CAPILLARY CHARGE" OF FLOATING PARTICLES

First of all, let us specify the sign of the capillary charge,

$$Q_k \equiv r_k \sin\psi_k, \tag{8.5}$$

which is a matter of convention. We will use the convention that the angle ψ_k is *positive* for *light* particles (Fig. 8.2a) and *negative* for *heavy* particles (Fig. 8.2b). Correspondingly, Q_k and h_k are positive for light particles and negative for heavy particles. The parameter b_k (k = 1,2) in Fig. 8.2 denotes the depth of immersion of the respective particle in the lower fluid (phase I). The volume of the part of the sphere, which is immersed in the lower fluid is

$$V_l^{(k)} = \pi b_k^2 (R_k - b_k/3), \qquad k = 1,2, \tag{8.6}$$

supposedly the contact line is horizontal. The radius of the contact line can be also expressed in terms of b_k :

$$r_k = [(2R_k - b_k)b_k]^{1/2}, \qquad k = 1,2. \tag{8.7}$$

As shown in Ref. [2], the gravitational force (particle weight + buoyancy force) exerted on a floating particle is

$$F_{g(k)} = g[(\rho_1 - \rho_k)V_l^{(k)} + (\rho_{1I} - \rho_k)V_u^{(k)} - \Delta\rho\,\pi r_k^2 h_k] \tag{8.8}$$

where $V_u^{(k)}$ denotes the upper part of particle volume, that immersed in phase II; as before ρ_{I} and ρ_{II} denote the mass densities of the fluid phases I and II, whereas ρ_k is the mass density of the k-th particle; $\Delta\rho \equiv \rho_{\mathrm{I}} - \rho_{\mathrm{II}}$. Note that Eq. (8.8) can be used not only for solid spheres, but also for fluid particles (drops, bubbles), like that in Fig. 2.3, which are composed of two axisymmetric segments, but are not spherical as a whole.

In the special case of spherical particle of radius R_k and volume $V_s^{(k)}$ one can write

$$V_u^{(k)} = V_s^{(k)} - V_l^{(k)}, \qquad V_s^{(k)} \equiv \tfrac{4}{3}\pi R_k^3 \tag{8.9}$$

Then Eq. (8.8) can be represented in the form [4]

$$F_{g(k)} = \sigma q^2 (V_l^{(k)} - D_k V_s^{(k)} - \pi r_k^2 h_k), \qquad (q^2 = \Delta\rho\, g/\sigma) \tag{8.10}$$

where

$$D_k \equiv \frac{\rho_k - \rho_{\mathrm{II}}}{\rho_{\mathrm{I}} - \rho_{\mathrm{II}}} \tag{8.11}$$

Combining Eqs. (8.1), (8.5), (8.6) and (8.10) one obtains an expression for the capillary charge [4]:

$$Q_k = \tfrac{1}{2} q^2 [b_k^2 (R_k - b_k/3) - \tfrac{4}{3} D_k R_k^3 - r_k^2 h_k] \tag{8.12}$$

By means of geometrical considerations from Fig. 8.2 one can deduce

$$\psi_k = \arccos\left(\frac{b_k}{R_k} - 1\right) - \alpha_k \qquad (k = 1,2) \tag{8.13}$$

Equations (7.56), (8.5), (8.7), (8.12) and (8.13) form a set of 10 equations for determining the 10 unknown parameters: Q_k, h_k, r_k, ψ_k and b_k (k = 1,2) for every value of the distance L between the two floating particles.

It turns out [3,4] that for small particles the capillary charge Q_k is a rather weak function of the distance L. For that reason one can obtain a convenient approximate formula for Q_k. With that end in view we first notice that the lower portion of particle volume can be expressed in the form

$$V_l^{(k)} = \tfrac{1}{3}\pi R_k^3 \left(2 + 3\cos\theta_k - \cos^3\theta_k\right), \qquad \theta_k = \arcsin(r_k/R_k) = \alpha_k + \psi_k. \tag{8.14}$$

Combining Eqs. (8.10) and (8.14) one derives

$$F_{g(k)} \approx \tfrac{1}{3}\pi\sigma q^2 R_k^3\left(2 - 4D_k + 3\cos\theta_k - \cos^3\theta_k\right), \qquad (qR_k << 1) \tag{8.15}$$

Here we have used the fact that for $qR_k << 1$ the term $\pi r_k^2 h_k$ in Eq. (8.10) can be neglected. In addition, for $qR_k << 1$ one can use the approximation $\theta_k \approx \alpha_k$. Then the combination of Eqs. (8.1) and (8.15) yields [3,4]

$$Q_k \approx Q_{k\infty} = \tfrac{1}{6} q^2 R_k^3\left(2 - 4D_k + 3\cos\alpha_k - \cos^3\alpha_k\right)\left[1 + O(qR_k)\right] \tag{8.16}$$

Equation (8.16) allows one to calculate the capillary charge Q_k directly from the particle radius R_k and contact angle α_k.

The capillary charge of a floating particle Q_k is a quantity of bounded variation. Indeed, from Eqs. (8.5) and (8.14) one can deduce that $Q_k = R_k \sin(\alpha_k + \psi_k) \sin\psi_k$. The condition for extremum of Q_k reads

$$0 = \frac{dQ_k}{d\psi_k} = R_k[\cos(\alpha_k + \psi_k)\sin\psi_k + \sin(\alpha_k + \psi_k)\cos\psi_k] = R_k \sin(\alpha_k + 2\psi_k) \tag{8.17}$$

Equation (8.17) has two roots of physical importance: $\psi_k = -\alpha_k/2$ and $\psi_k = (\pi - \alpha_k)/2$; they determine the minimum and maximum values of Q_k [4,5]:

$$-R_k \sin^2(\alpha_k/2) \le Q_k \le R_k \cos^2(\alpha_k/2) \tag{8.18}$$

For $Q_k < -R_k \sin^2(\alpha_k/2)$ the particle would sink into the lower phase I; on the other hand, for $Q_k > R_k \cos^2(\alpha_k/2)$ the particle would enter the upper phase II. In particular, if the contact angle is $\alpha_k = 0$, then Eq. (8.18) implies $Q_k \ge 0$, that is only light particles can attach to the interface (heavy particles with $Q_k < 0$ would sink into phase I).

8.1.3. COMPARISON BETWEEN THE CAPILLARY FLOTATION AND IMMERSION FORCES

Equations (7.13) and (8.4), and their asymptotic form for $qL << 1$,

$$F = -2\pi\sigma\frac{Q_1 Q_2}{L} \qquad r_k << L << q^{-1} \tag{8.19}$$

(q^{-1} = 2.7 mm for water), show that the immersion and flotation forces exhibit the same functional dependence on the interparticle distance L. On the other hand, the "capillary

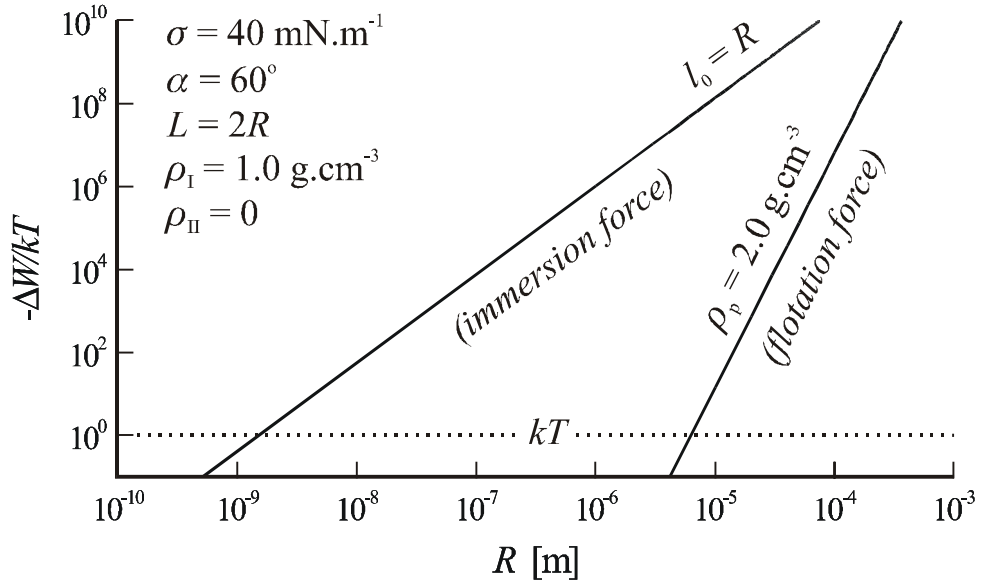

Fig. 8.3. Energy of capillary attraction ΔW, in kT units, plotted vs. the radius R of two similar particles separated at a center-to-center distance $L = 2R$. If $\Delta W > kT$, the capillary attraction is stronger than the Brownian force and can cause a two-dimensional aggregation of the particles [4,6].

charges", Q_1 and Q_2, can be very different for these two kinds of capillary force. To demonstrate that let us consider the case of two identical particles, for which $R_1 = R_2 = R$ and $\alpha_1 = \alpha_2 = \alpha$; then using Eqs. (8.5) and (8.16) one can derive [4,6,7]

$$\begin{aligned} &F \propto \left(R^6/\sigma\right)\mathrm{K}_1(qL) \quad \text{for flotation force} \\ &F \propto \sigma R^2 \mathrm{K}_1(qL) \quad \text{for immersion force} \end{aligned} \tag{8.20}$$

Consequently, the flotation force decreases, while the immersion force increases, when the interfacial tension σ increases. Besides, the flotation force decreases much stronger with the decrease of particle radius R than the immersion force. Thus $F_{\text{flotation}}$ is negligible for $R < 5$–10 μm, whereas $F_{\text{immersion}}$ can be significant even for $R = 2$ nm [4,6]. This is illustrated in Fig. 8.3, where the two types of capillary interaction are compared, with respect to their energy $\Delta W(L) = \int_L^\infty F(L')dL'$, for a wide range of particle sizes. The values of the parameters used are: particle mass density $\rho_p = 2$ g/cm^3, density difference between the two fluids $\Delta\rho = 1$ g/cm^3, surface tension $\sigma = 40$ mN/m, contact angle $\alpha = 60°$, interparticle distance $L = 2R$, and

thickness of the non-disturbed planar film $l_0 = R$. Protein molecules of nanometer size can be considered as "particles" insofar as they are much larger than the solvent (water) molecules. For example, the radius of a water molecule is about 0.12 nm; then a protein of radius $R \geq 1.2$ nm can be considered as being much larger.

The pronounced difference in the strength of the two types of capillary interactions, see Fig. 8.3, is due to the different magnitude of the interfacial deformation. The small floating particles are too light to create a substantial deformation of the liquid surface and then the lateral capillary force becomes negligible. In the case of immersion forces the particles are restricted in the vertical direction by the solid substrate (see Fig. 7.1b) or by the two surfaces of the liquid film (Fig. 7.1f). Therefore, as the film becomes thinner, the liquid surface deformation increases, thus giving rise to a strong interparticle attraction. For that reason, as already mentioned, the immersion forces may be one of the main factors causing the observed self assembly of μm-sized and sub-μm colloidal particles and protein macromolecules confined in thin liquid films or lipid bilayers.

In conclusion, the different physical origin of the flotation and immersion lateral capillary forces results in different magnitudes of the "capillary charges" Q_k, which depend in a different way on the interfacial tension σ and the particle radius R, see Eqs. (8.4) and (8.20). In this respect these two kinds of capillary force resemble the electrostatic and gravitational forces, which obey the same power law, but differ in the physical meaning and magnitude of the force constants (charges, masses) [7,8].

8.1.4. More accurate calculation of the capillary interaction energy

To derive Eq. (8.2) we have used the superposition approximation, i.e. we approximately presented the meniscus around two floating particles as a superposition of the axisymmetric menisci around each particle in isolation. Although this approximation works well for long interparticle separations, at short distances it is not quantitatively correct; in particular, it leads to violation of the boundary condition for constancy of the contact angle at the particle surface (the Young equation). We can overcome this problem using the more rigorous expressions derived in Section 7.2 by means of bipolar coordinates. Second problem with the superposition

approximation is that the interaction energy is assumed to be identical to the gravitational energy of one of the two floating particles, thus apriori neglecting the contributions of the meniscus surface energy and the energy of wetting. The latter assumption needs to be verified and validated. The above two issues are elucidated below following Ref. [4].

Gravitational, wetting and meniscus contributions. Our starting point are Eqs. (7.16)–(7.18) which express the energy of the system (the grand thermodynamic potential) Ω as a sum of gravitational, wetting and meniscus contributions, $\Omega = W_g + W_w + W_m$. The meniscus surface energy is given again by Eq. (7.93), which can be represented in the form

$$\Delta W_m = W_m - W_{m\infty} = \pi\sigma \sum_{k=1,2} \left(Q_k h_k - r_k^2 \right) - \Delta\rho g I_v - W_{m\infty} , \tag{8.21}$$

where $W_{m\infty}$ is the limiting value of W_m for infinite interparticle separation ($L\to\infty$); I_v is given by Eq. (7.72). Substituting the geometrical expressions for the portions of the particle area wet by fluids I and II in Eq. (7.18) one obtains [4]:

$$W_w = 2\pi \sum_{k=1,2} [\sigma_{k,I} R_k b_k + \sigma_{k,II} R_k (2R_k - b_k)] \tag{8.22}$$

Using the Young equation, $\sigma_{k,II} - \sigma_{k,I} = \sigma \cos\alpha_k$, and the fact that the particle radius R_k is independent of L from Eq. (8.22) one obtains

$$\Delta W_w = -2\pi\sigma \sum_{k=1,2} R_k b_k \cos\alpha_k - W_{w\infty} \tag{8.23}$$

where $W_{w\infty}$ is the limiting value of the first term in the right-hand side of Eq. (8.23) for $L\to\infty$. ΔW_w expresses the contribution of wetting to the capillary interaction energy. Finally, using Eq. (7.17) and geometrical considerations for the system depicted in Fig. 8.2 one can derive the gravitational contribution to the capillary interaction energy [4]:

$$\Delta W_g = \Delta\rho g \{ I_v + \sum_{k=1,2} [(D_k V_s^{(k)} - V_l^{(k)}) Z_k^{(c)} + \pi(r_k^2 + 2h_k^2) r_k^2/4] \} - W_{g\infty} \tag{8.24}$$

where $W_{g\infty}$ is the limiting value of W_g for $L\to\infty$, and

$$Z_k^{(c)} = h_k - b_k + R_k \qquad (k = 1,2) \tag{8.25}$$

is the z-coordinate of the (mass) center of the k-th sphere. Note that when summing up Eqs. (8.21) and (8.24) the terms with I_v cancel each other. In view of Eq. (7.16) the total energy of capillary interaction between two floating particles can be expressed in the form [4]

$$\Delta\Omega = \Delta W_w + \Delta\widetilde{W}_m + \Delta\widetilde{W}_g \tag{8.26}$$

where ΔW_w is given by Eq. (8.23); $\Delta\widetilde{W}_m$ and $\Delta\widetilde{W}_g$ are defined without the canceling I_v-term as follows

$$\Delta\widetilde{W}_m = \pi\sigma \sum_{k=1,2} \left(Q_k h_k - r_k^2\right) - \tilde{W}_{m\infty} \tag{8.27}$$

$$\Delta\widetilde{W}_g = -\pi\sigma \sum_{k=1,2} \left\{2Q_k h_k - q^2[\tfrac{1}{4}(r_k^2 - 2h_k^2)r_k^2 + (\tfrac{4}{3}D_k R_k^3 - R_k b_k^2 + \tfrac{1}{3}b_k^3)(R_k - b_k)]\right\} - \widetilde{W}_{g\infty} \tag{8.28}$$

To obtain Eq. (8.28) from Eq. (8.24) we have used Eqs. (8.6), (8.9) and (8.25); the constants $\widetilde{W}_{m\infty}$ and $\widetilde{W}_{g\infty}$ are defined in such a way that for $L\to\infty$ both $\Delta\widetilde{W}_m$ and $\Delta\widetilde{W}_g$ tend to zero.

Asymptotic expression for the capillary flotation force. It has been proven by Chan et al. [3] that when the particles are small, the meniscus slope is also small, that is

$$(qR_k)^2 << 1 \quad \Rightarrow \quad \sin^2\psi_k << 1 \qquad (k = 1,2) \tag{8.29}$$

Combining the latter relationships with Eqs. (7.51) and (8.16) one can derive [4]:

$$|Q_k|/R_k \sim (qR_k)^2 << 1, \qquad |h_k/R_k| \sim (qR_k)^2\,|\ln(qR_k)| << 1, \qquad (k = 1,2) \tag{8.30}$$

As demonstrated in Appendix 8A Eqs. (8.29) and (8.30) imply

$$\frac{db_k}{dL} = -r_k \frac{d\psi_k}{dL} = -\frac{dQ_k}{dL}[1 + O(q^2 R_k^2)] = \tfrac{1}{2}(qr_k)^2 \frac{dh_k}{dL}[1 + O(q^2 R_k^2)] \tag{8.31}$$

A differentiation of Eqs. (8.23), (8.27) and (8.28), along with Eqs. (8.7) and (8.31) yields [4]:

$$\frac{d\Delta W_w}{dL} = -\pi\sigma \sum_{k=1,2} (qr_k)^2 R_k \cos\alpha_k \frac{dh_k}{dL}[1 + O(q^2 R_k^2)] \tag{8.32}$$

$$\frac{d\Delta\widetilde{W}_m}{dL} = \pi\sigma \sum_{k=1,2} [Q_k + (qr_k)^2 R_k \cos\alpha_k] \frac{dh_k}{dL}[1 + O(q^2 R_k^2)] \tag{8.33}$$

$$\frac{d\Delta\widetilde{W}_{\mathrm{g}}}{dL} = -\pi\sigma \sum_{k=1,2} 2Q_k \frac{dh_k}{dL}[1 + O(q^2 R_k^2)] \tag{8.34}$$

Finally, in view of Eq. (8.26) we sum up Eqs. (8.32)–(8.34) to obtain an expression for the capillary flotation force between small particles [4]:

$$F = -\frac{d\Delta\Omega}{dL} = \pi\sigma \sum_{k=1,2} Q_k \frac{dh_k}{dL}[1 + O(q^2 R_k^2)] \tag{8.35}$$

The form of Eqs. (8.32)–(8.35) calls for some discussion. First, one sees that the contributions of the wetting, meniscus surface and gravitational energies have comparable magnitudes. However, when deriving the expression for F the derivative $d(\Delta W_{\mathrm{w}})/dL$ is canceled by a part of $d(\Delta\widetilde{W}_{\mathrm{m}})/dL$, and the result represents a half of the gravitational contribution $d(\Delta\widetilde{W}_{\mathrm{g}})/dL$. Thus, in a final reckoning, F turns out to be (approximately) equal to the half of the gravitational contribution, just as assumed by Nicolson long ago [1], see Section 8.1.1.

Equation (8.31) shows that the dependence of Q_k on L is rather weak; then the integration of Eq. (8.35) can be formally carried out at constant Q_k [4]:

$$\Delta\Omega = -\pi\sigma \sum_{k=1,2} (Q_k h_k - Q_{k\infty} h_{k\infty})[1 + O(q^2 R_k^2)] \tag{8.36}$$

The substitution of some of the expressions for h_k derived in Section 7.2.2 in Eqs. (8.35) and (8.36) allow one to calculate the dependencies $F(L)$ and $\Delta\Omega(L)$. More details about the procedure of calculation are given in the next section 8.1.5. In particular, from Eqs. (8.35) and (8.36), along with Eq. (7.56), one recovers the asymptotic expressions

$$F = -2\pi\sigma Q_1 Q_2 q \mathrm{K}_1(qL)[1 + O(q^2 R_k^2)], \qquad r_k << L, \tag{8.37}$$

$$\Delta\Omega = -2\pi\sigma Q_1 Q_2 \mathrm{K}_0(qL)[1 + O(q^2 R_k^2)], \qquad r_k << L. \tag{8.38}$$

8.1.5. NUMERICAL RESULTS AND DISCUSSION

Procedure of calculations. The derived equations enable one to calculate the energy and force of capillary interaction between two floating particles, $\Delta\Omega$ and F. The input parameters are usually the interfacial tension σ, the capillary length q^{-1}, the density ratio D_k, the contact angle α_k, the particle radius R_k (k = 1,2), and the interparticle distance L.

The remaining 10 parameters, Q_k, h_k, r_k, ψ_k and b_k (k = 1,2) can be determined for every value of the distance L between the two floating particles using the set of Eqs. (7.48), (8.5), (8.7), (8.12) and (8.13). For longer distances between the particles ($L >> r_k$) the usage of Eq. (7.56) is recommended instead of Eq. (7.48).

For $R_k \leq 850$ μm one can use a much faster iteration procedure proposed in Ref. [4]. Since for small particles the meniscus slope is also small, $\sin^2\psi_k << 1$, cf. Eq. (8.29), one can write

$$r_k = R_k \sin(\alpha_k + \psi_k) \approx R_k \cos\alpha_k \sin\psi_k + R_k \sin\alpha_k \tag{8.39}$$

In view of Eq. (8.5) one can substitute $\sin\psi_k = Q_k/r_k$ and then Eq. (8.39) transforms into a quadratic equation for r_k, whose solution reads

$$r_k = \tfrac{1}{2}\,[R_k \sin\alpha_k + (R_k^2 \sin^2\alpha_k + 4Q_k R_k \cos\alpha_k)^{1/2}] \tag{8.40}$$

Next, from Eq. (8.31) one obtains

$$Q_k^{(n+1)} = Q_k^{(n)} - \tfrac{1}{2}(qr_k)^2 (h_k^{(n+1)} - h_k^{(n)}) \qquad (k = 1,2) \tag{8.41}$$

where $Q_k^{(n+1)}$ and $Q_k^{(n)}$ are two consecutive approximations for Q_k, as well as $h_k^{(n+1)}$ and $h_k^{(n)}$ are two consecutive approximations for h_k; n = 0, 1, 2,... . The iteration procedure has the following steps [4]:

(i) As a zeroth-order approximation one can use

$$r_k^{(0)} = r_{k\infty}, \qquad Q_k^{(0)} = Q_{k\infty}, \qquad h_k^{(0)} = h_{k\infty}, \tag{8.42}$$

where $Q_{k\infty}$ is determined from Eq. (8.16), $r_{k\infty}$ is then calculated from Eq. (8.40) and $h_{k\infty}$ is determined from Eq. (7.51).

(ii) $h_k^{(n+1)}$ is calculated from Eq. (7.48) [or Eq. (7.56) for $L >> r_k$] substituting $Q_k = Q_k^{(n)}$ and $r_k = r_k^{(n)}$.

(iii) Then from Eq. (8.41) one obtains the next approximation, $Q_k^{(n+1)}$, which is to be substituted in Eq. (7.40) to get $r_k^{(n+1)}$. Next, step (ii) is repeated again to give $h_k^{(n+2)}$, etc.

This iteration procedure is quickly convergent when $(qr_k)^2$ in Eq. (8.41) is a small parameter. With the values of Q_k, r_k and h_k thus obtained one next calculates ψ_k and b_k:

$$\psi_k = \arcsin(Q_k/r_k), \qquad b_k = R_k[1 + \cos(\alpha_k + \psi_k)]. \tag{8.43}$$

Finally, from Eqs. (8.23) and (8.26)–(8.28) one determines the energy of capillary interaction $\Delta\Omega(L)$; the capillary flotation force can be obtained by differentiation: $F = -d(\Delta\Omega)/dL$. For $R_k \leq 100$ μm one can calculate $\Delta\Omega$ and F from Eqs. (8.35) and (8.36). Note that the latter two equations are more general than Eqs. (8.37) and (8.38) which are subject to the additional restriction $L >> r_k$.

Calculated energy and force of capillary interaction. The capillary force, $F = -d(\Delta\Omega)/dL$, calculated by numerical differentiation of Eq. (8.26) [along with Eqs. (7.48), (8.23), (8.27) and (8.28)], can be compared with the capillary force calculated from the asymptotic formula, Eq. (8.37), along with Eq. (8.16). For that purpose the ratio, Φ, of the values of F calculated by means of the more rigorous and less rigorous equations,

$$\Phi = \frac{F(\text{Eq.(8.26)})}{F(\text{Eq.(8.37)})}\ , \tag{8.44}$$

has been calculated as a function of the interparticle distance L. Figure 8.4 shows plots of Φ vs. $L/2R$ obtained in Ref. [4] for two identical floating particles using the following parameter values: $R_1 = R_2 = R = 10$ μm, $\rho_1 = \rho_2 = 3$ g/cm^3; water-air interface : $\rho_{\text{I}} = 1$ g/cm^3, $\rho_{\text{II}} = 0$, $\sigma = 70$ mN/m. The three curves in Fig. 8.4 correspond to three different values of the particle contact angle: $\alpha_1 = \alpha_2 = \alpha = 30°$, 60° and 90°.

For $L/2R > 3$ one has $\Phi \approx 1$, that is the two equations predict practically identical values of the force F, see Fig. 8.4. This result could be anticipated, because Eq. (8.37) is an asymptotic expression for the capillary force derived for the case of large interparticle separations. On the other hand, Fig. 8.4 shows that for shorter distances ($L/2R < 2$) and for $\alpha > 30°$ the asymptotic formula, Eq. (8.37), considerably underestimates the capillary force; hence in such cases the usage of the more rigorous Eq. (8.26) has to be recommended for calculation of F.

Figure 8.5 shows plot of $\Delta\Omega/kT$ vs. L calculated by means of Eq. (8.26) for two *identical* particles. The temperature is 25°C; the values of the other parameters are shown in the figure.

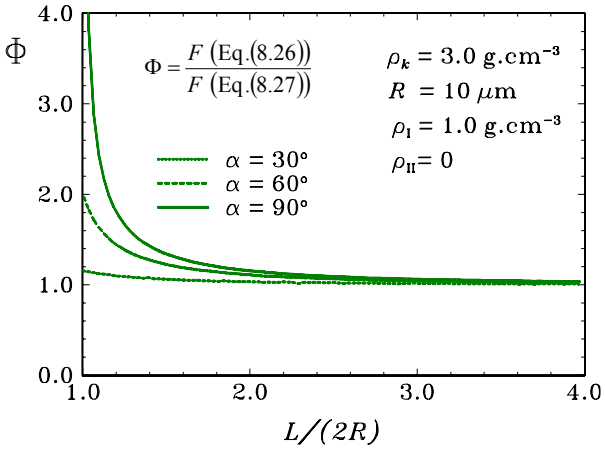

Fig. 8.4. Plot of Φ vs. distance L scaled by the particle diameter $2R$ obtained in Ref. [4] for two identical particles; Φ is the ratio of the values of the capillary force calculated by means of the more rigorous Eq. (8.26) and the approximate Eq. (8.37).

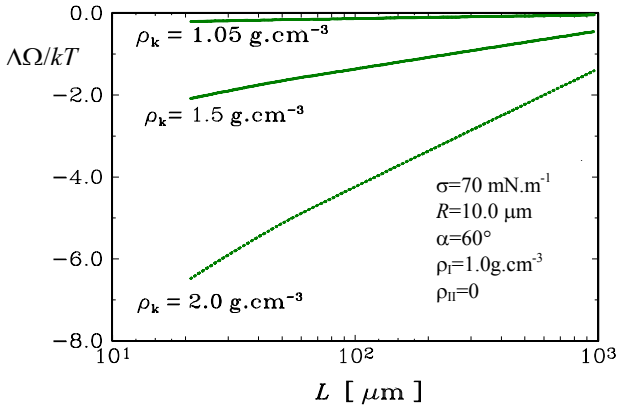

Fig. 8.5. Dependence of the capillary interaction energy $\Delta\Omega/kT$ on the distance L between two identical floating particles calculated in Ref. [4] for three different values of the particle mass density ρ_k.

The curves in Fig. 8.5 are close to straight lines, which can be explained with the fact that Eqs. (7.54) and (8.38) predict $\Delta\Omega \propto \ln(qL)$ for $qL << 1$; note that L is plotted in log scale along the abscissa of Fig. 8.5. In addition, in Fig. 8.5 one sees that for such small particles (R = 10 μm) the energy of capillary attraction due to the flotation force is relatively small, not larger than several kT, and increases markedly with the rise of the particle density ρ_k.

For the couple of particles, whose density (ρ_k = 1.05 g/cm^3) is close to that of the lower fluid phase (ρ_l = 1 g/cm^3) $\Delta\Omega$ is smaller than the thermal energy kT, and in this case the capillary attraction between the particles is negligible.

Figure 8.6 illustrates the fact that for two identical particles the dependence of the energy of capillary attraction, $\Delta\Omega$, on the particle mass density, ρ_k, is a non-monotonic one. Qualitatively, this can be easily anticipated, because for light and heavy particles one has the configurations depicted in Figs. 8.2a and 8.2b, respectively, corresponding to positive and negative meniscus slope angle ψ_k. Then for some intermediate value of the particle density ρ_k* the slope angle becomes $\psi_k = 0$, which means that there is no interfacial deformation and capillary attraction; the latter situation corresponds to the upper points (with $\Delta\Omega = 0$) of the curves in Fig. 8.6.

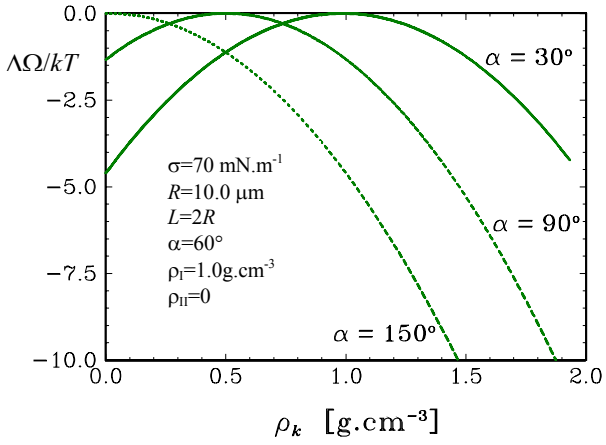

Fig. 8.6. Plot of the capillary interaction energy $\Delta\Omega/kT$ vs. particle mass density ρ_k calculated in Ref. [4] for three different values of the contact angle α of two identical spherical particles of radius R = 10 μm separated at a distance $L = 2R$.

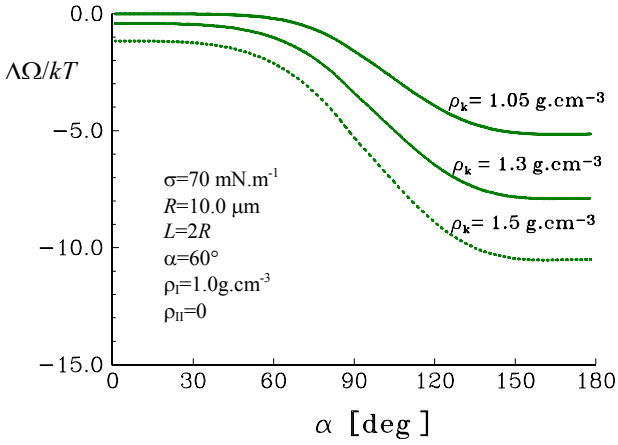

Fig. 8.7. Plot of the capillary interaction energy $\Delta\Omega/kT$ vs. contact angle α calculated in Ref. [4] for three different values of the mass density ρ_k of two identical spherical particles of radius R = 10 μm separated at a distance $L = 2R$.

Since for $\psi_k = 0$ one has $Q_k = 0$, we can estimate the value of ρ_k* from Eqs. (8.11) and (8.16):

$$\frac{\rho_k^* - \rho_{II}}{\rho_I - \rho_{II}} = \tfrac{1}{4}(2 + 3\cos\alpha_k - \cos^3\alpha_k) \tag{8.45}$$

In particular, for $\alpha_k = 90°$, $\rho_I = 1$ g/cm^3 and $\rho_{II} = 0$ Eq. (8.45) predicts ρ_k* = 0.5 g/cm^3 which exactly corresponds to the maximum of the curve with $\alpha = 90°$ in Fig. 8.6.

Figure 8.7 shows plots of $\Delta\Omega/kT$ vs. α, calculated in Ref. [4], which illustrate the dependence of the capillary interaction energy on the contact angle; the three curves correspond to three different values of the particle mass density ρ_k (two identical particles, $\alpha \equiv \alpha_k$). The values of the other parameters in Fig. 8.7 are the same as in Fig. 8.6. One sees in Fig. 8.7 that the dependence of $\Delta\Omega$ on α is the most pronounced in the interval $45° < \alpha < 135°$, whereas outside this interval $\Delta\Omega$ is almost constant. This behavior can be attributed to the fact that the capillary charge Q_k depends on $\cos\alpha_k$, see Eq. (8.16), and $\cos\alpha_k$ varies strongly in the interval $45° < \alpha < 135°$, while it is almost constant ($\cos\alpha_k \approx \pm 1$) outside this interval.

Figure 8.8 shows plots of $\Delta\Omega/kT$ vs. σ, calculated in Ref. [4], which illustrate the dependence of the capillary interaction energy on the value of the interfacial tension (case of two identical

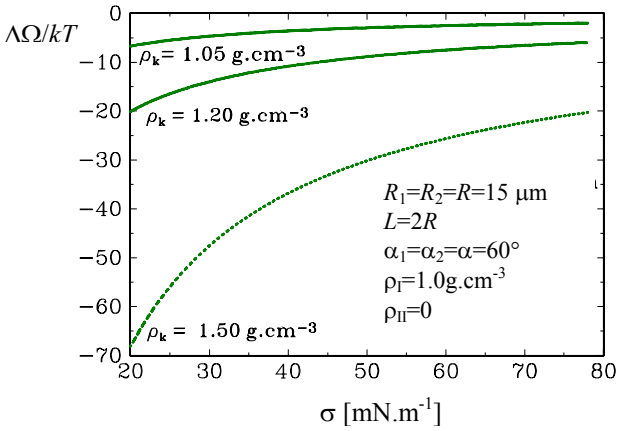

Fig. 8.8. Plot of the capillary interaction energy $\Delta\Omega/kT$ vs. interfacial tension σ calculated in Ref. [4] for three different values of the mass density ρ_k of two identical spherical particles of radius R = 15 μm and contact angle α_k = 60° separated at a distance $L = 2R$.

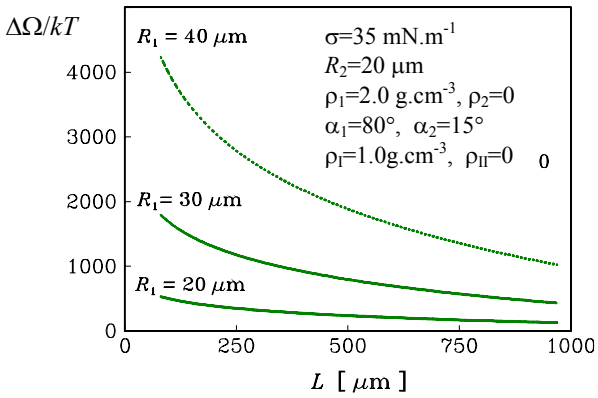

Fig. 8.9. Plot of the energy of capillary repulsion $\Delta\Omega/kT$ vs. distance L between a heavy particle of radius R_1 and a light particle (bubble) of radius R_2 = 20 μm; the curves are obtained in Ref. [4] for three different values of R_1.

particles). One sees that the lower the interfacial tension σ, the greater the magnitude of the interaction energy $|\Delta\Omega|$. To understand this behavior one first notices that $q^2 \propto 1/\sigma$ and then Eq. (8.16) gives $Q_k \propto 1/\sigma$. Then in accordance with Eq. (8.38) one can write $\Delta\Omega \propto \sigma Q_k^2 \propto 1/\sigma$, which explains the trend of the curves in Fig. 8.8. From a physical viewpoint this means that when the interfacial tension σ is smaller, a floating heavy (or light) particle creates a larger surface deformation ($\sin\psi_k \propto Q_k$), which gives rise to a stronger capillary attraction if the menisci formed around two such particles overlap. This behavior of the dependence $\Delta\Omega$ vs. σ has been first theoretically established by Chan et al. [3] for the case of *flotation* forces. Note, however, that in the case of immersion force the trend is exactly the opposite: $\Delta\Omega$ grows with the increase of σ, i.e. $\Delta\Omega \propto \sigma$, see Eq. (8.20) and Ref. [6].

Up to here, all considered numerical examples (Figs. 8.4–8.8) correspond to the case of two identical particles, which experience attractive capillary force. The derived equations enable one to obtain theoretical results also for the case of two *non-identical* particles, which may experience *repulsive* capillary force. As an example, in Fig. 8.9 we give the plot of $\Delta\Omega/kT$ vs. L for a couple of dissimilar particles: a heavy particle of mass density ρ_1 = 2 g/cm^3 and a hollow sphere (bubble) of mass density ρ_2 = 0; the values of the other parameters are shown in the

figure. The configuration resembles that in Fig. 7.1c and one could expect that the interaction between the two dissimilar particles will be repulsive. The three curves in Fig. 8.9, calculated in Ref. [4] for three values of the radius of the heavy particle, R_2 = 20, 30 and 40 μm, really correspond to $\Delta\Omega > 0$, i.e. to repulsion.

Note also that the magnitude of the interaction energy in Fig. 8.9 is much greater that that in Fig. 8.5. The reason is that the particle radii in Fig. 8.9 are larger than those in Fig. 8.5, and that the capillary flotation force increases very strongly with the rise of the particle size: $\Delta\Omega \propto Q_1 Q_2 \propto R_1^3 R_2^3$, see Eqs. (8.16) and (8.38). Thus for two identical particles, $R_1 = R_2 = R$, one obtains $\Delta\Omega \propto R^6$ and $F \propto R^6$, cf. Eqs. (8.20) and (8.37). This strong dependence of the flotation force on the particle size makes it to vanish for Brownian particles of radius $R \leq 1$ μm, see Fig. 8.3. In other words, the *flotation* force turns out to be an essentially macroscopic effect. On the other hand, the *immersion* force is operative between both sub-micrometer (Brownian) and larger particles.

8.2. PARTICLE-WALL INTERACTION: CAPILLARY IMAGE FORCES

8.2.1. ATTRACTIVE AND REPULSIVE CAPILLARY IMAGE FORCES

In this section we consider a particle of radius in the range between 5 μm and 1 mm, which is floating on a liquid surface in the vicinity of a vertical wall. The overlap of the meniscus around the floating particle with the meniscus on a vertical wall gives rise to a particle-wall interaction, which can be both repulsive and attractive, as explained below. We will use subscripts "1" and "2" to denote parameters characterizing the wall and particle, respectively.

First, following Refs. [9,10], we consider the simplest case, when the contact angle at the wall is $\alpha_1 = 90°$. In such a case the meniscus would be flat if the floating particle (Fig. 8.10a) were removed. Let us denote by $\zeta_0(x,y)$ the meniscus shape in the presence of particle. Since $\alpha_1 = 90°$, the function $\zeta_0(x,y)$ must satisfy the boundary condition $(\partial\zeta_0/\partial x)_{x=0} = 0$ at the wall surface. Using considerations for symmetry one realizes that the meniscus shape $\zeta_0(x,y)$ in Fig. 8.10a would be the same if (instead of a wall at a distance s) one has a second particle (mirror image) floating at a distance $2s$ from the original particle. The "image" must be identical to the original particle with respect to its size, weight and contact angle; in other words,

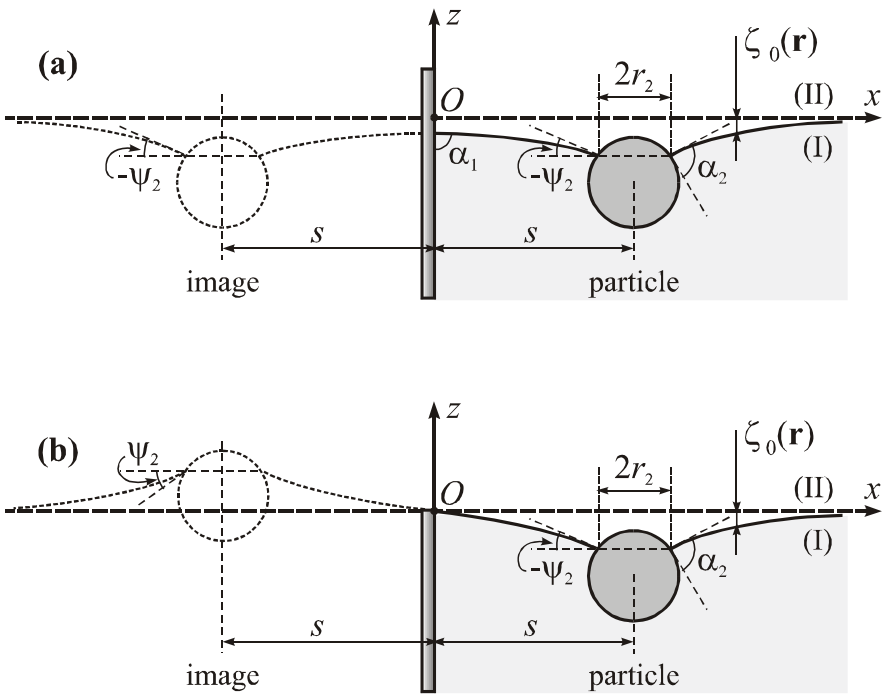

Fig. 8.10. Sketch of the meniscus profile, $\zeta_0(\mathbf{r})$, around a particle floating in the vicinity of a vertical wall; α_2 and r_2 are the particle contact angle and contact line radius; ψ_2 is the meniscus slope angle at the particle contact line; (a) fixed contact angle at the wall ($\alpha_1 = 90°$) corresponding to attractive capillary image force; (b) fixed contact line at the wall ($\zeta_0 \equiv 0$ for $x = 0$) which leads to repulsive capillary image force [9].

the particle and its image have identical "capillary charges", equal to Q_2. Note, that the capillary charge of the floating particle can be estimated by means of Eq. (8.16) above. As mentioned earlier, the lateral capillary force between two identical particles is always attractive. Hence, the particle and its mirror image depicted in Fig. 8.10a will attract each other, which in fact means that the wall will attract the floating particle; the resulting force will (asymptotically) obey Eq. (8.37) with $Q_1 = Q_2$.

The boundary condition $\zeta_0(x=0) = 0$ represents a requirement for a zero elevation of the contact line at the wall. As noticed in Ref. [9] this can be experimentally realized if the contact line is attached to the edge of a vertical plate, as shown in Fig. 8.10b, or to the boundary between a hydrophobic and a hydrophilic domain on the wall. As before, we assume that the meniscus would be flat if the floating particle (Fig. 8.10b) were removed. Using again considerations for symmetry, one realizes that the meniscus shape $\zeta_0(x,y)$ in Fig. 8.10b would be the same if

(instead of a wall at a distance s) one has a second particle (image) of the *opposite* capillary charge ($Q_1 = -Q_2$) at a distance $2s$ from the original particle. In such a case the capillary force is repulsive, i.e. in reality the wall will repel the floating particle [9].

The above considerations imply that one can use Eq. (8.37) with $L = 2s$ to describe the asymptotic behavior of the particle-wall interaction for the two configurations depicted in Figs. 8.10a and 8.10b:

$$F = (-1)^{\lambda}\, 2\pi\sigma\, Q_2^2\, q\mathrm{K}_1(2qs)[1 + O(q^2 R_k^2)], \qquad r_k << L, \tag{8.46}$$

where

$$\lambda = \begin{cases} 1 & \text{for fixed contact angle at the wall;} \\ 0 & \text{for fixed contact line at the wall.} \end{cases} \tag{8.47}$$

Such capillary interactions between a floating particle and a vertical wall, which are equivalent to the interaction between the particle and its mirror image, are termed "capillary image forces" in Ref. [9]. In fact, they resemble the electrostatic image forces, appearing when an electric charge imbedded in a medium of dielectric permittivity ε_1 is located in the neighborhood of a boundary with a second medium of permittivity ε_2. The electrostatic image force is proportional to the difference $(\varepsilon_1 - \varepsilon_2)$, see e.g. [11,12], and consequently, this force can be repulsive or attractive depending on whether $\varepsilon_1 > \varepsilon_2$ or $\varepsilon_1 < \varepsilon_2$.

Coming back to the capillary image forces, we notice that the configurations depicted in Fig. 8.10 represent a very special case, insofar as we have assumed that the interface is horizontal in the absence of floating article ($\alpha_1 = 90°$). The usual experimental situation is that an inclined meniscus ($\alpha_1 \neq 90°$) is formed in a vicinity of the vertical wall. Below, following Ref. [9], we consider that more general case.

8.2.2. THE CASE OF INCLINED MENISCUS AT THE WALL

Qualitative dependence of energy vs. distance. Figure 8.11a shows the capillary meniscus formed in the neighborhood of a vertical planar wall. Now the contact angle α_1 at the wall is different from 90°. In such case, the gravitational force will tend to slip the particle

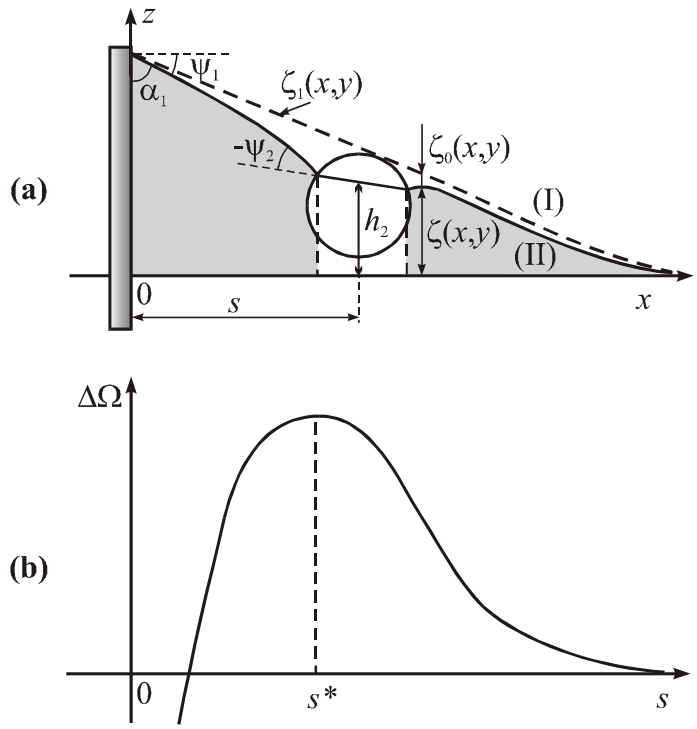

Fig. 8.11. (a) Sketch of a heavy particle floating at a distance s from a vertical wall of fixed three-phase contact angle $\alpha_1 < 90°$; $\zeta_1(x)$ is the non-disturbed meniscus of the wall and $\zeta_0(x,y)$ is the interfacial perturbation caused by the particle. (b) Typical dependence of the capillary interaction energy $\Delta\Omega$ vs. distance s corresponding to the above configuration of floating particle and wall [9].

along the inclined meniscus. We will restrict our considerations to the case of small meniscus slope,

$$\sin^2 \psi_1 << 1, \qquad (\psi_1 = 90° - \alpha_1) \tag{8.48}$$

(otherwise the gravitational force will be predominant and the effect of the lateral capillary force becomes negligible). Equation (8.48) corresponds to the nontrivial case, in which the total force exerted on the particle is an interplay of the gravitational effect (particle weight + buoyancy force) and the effect of the capillary image force. Prior to any quantitative considerations one can anticipate qualitatively the trend of the particle-wall interaction:

In Fig. 8.11a the contact angle $\alpha_1 < 90°$ is assumed constant, but the contact line on the wall is mobile. In such a case (like in Fig. 8.10a) the capillary image force is attractive, whereas the gravitational force will push the particle away from the wall. If the particle is large enough, the capillary image force will prevail at short distances, whereas the gravitational force will prevail

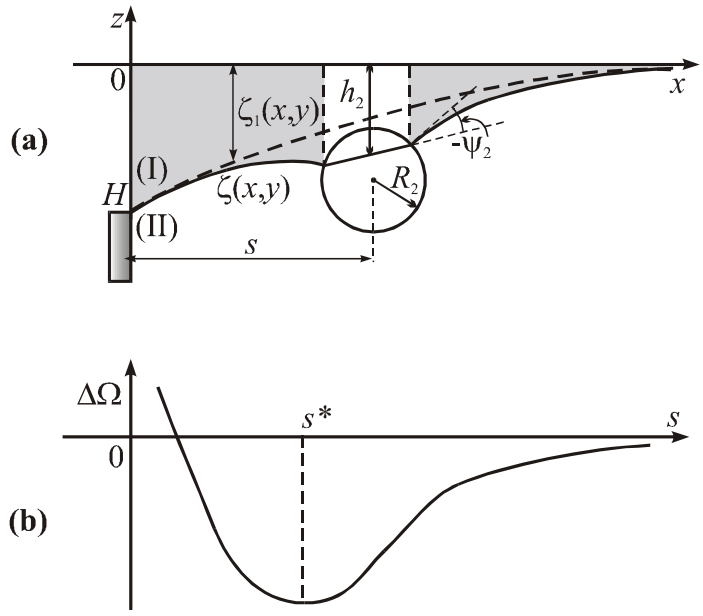

Fig. 8.12. (a) Sketch of a heavy particle of radius R_2 floating at a distance s from a vertical wall; the three-phase contact line is fixed at the edge of the wall, which is situated at the level $z = H$ below the horizontal liquid surface $z = 0$ far from the wall. $\zeta_1(x)$ is the non-disturbed meniscus of the wall and $\zeta_0(x,y)$ is the interfacial perturbation caused by the particle. (b) Typical dependence of the capillary interaction energy $\Delta\Omega$ vs. distance s corresponding to the above configuration of floating particle and wall [9].

at long distances. Therefore, one can expect that at some distance $s = s^*$ these two forces will counterbalance each other and the energy of the particle $\Delta\Omega$ will exhibit a maximum when plotted vs. the distance s, see Fig. 8.11b.

If the slope of the meniscus at the wall has the opposite sign, i.e. $\alpha_1 > 90°$ and $\psi_1 < 0$, then the plot of $\Delta\Omega$ vs. s for a heavy particle ($Q_2 < 0$) will be a monotonically increasing curve, because in this case both the gravitational and the capillary image force will have a tendency to bring the particle closer to the wall.

From a physical (including experimental) viewpoint more interesting is the case presented in Fig. 8.12: the position of the contact line is fixed at the edge of a plate or to the boundary between hydrophilic and hydrophobic regions on the wall. As mentioned above, in this case the capillary image force is repulsive. Let us denote by H the z-coordinate of the contact line on the wall; the choice of the coordinate system is shown in Fig. 8.12a, where $H < 0$. In such a case, the gravitational force will tend to bring a floating heavy particle (with $Q_2 < 0$) closer to the wall. Then at some separation $s = s^*$ the gravitational and the capillary image forces can

counterbalance each other and the particle will have a stable equilibrium position, corresponding to a minimum of the energy $\Delta\Omega$ (Fig. 8.12b). The dependence of $\Delta\Omega$ vs. s is similar if $H > 0$ and the particle is light ($Q_2 > 0$). The existence of a minimum of $\Delta\Omega$ at $s = s^*$ allows one to determine experimentally the dependence of s^* on H and thus to verify the theoretical predictions, see Section 8.2.7 below.

Shape of the contact line on the particle surface. As in Chapter 7, to quantify the capillary interaction we have to solve the Laplace equation and to determine the meniscus shape. Since we assume small meniscus slope, the Laplace equation can be linearized, see Eq. (7.6), and the solution $z = \zeta(x,y)$ can be formally expressed as a sum of the meniscus $\zeta_1(x)$ formed at the wall in the absence of a floating particle, and the deformation $\zeta_0(x,y)$ created by the particle in the absence of inclined meniscus at the wall ($\psi_1 = 0$, see Fig. 8.10) [9]:

$$\zeta(x,y) = \zeta_0(x,y) + \zeta_1(x). \tag{8.49}$$

Both $\zeta_0(x,y)$ and $\zeta_1(x)$ satisfy the linearized Laplace equation of capillarity:

$$\frac{\partial^2\zeta_0}{\partial x^2} + \frac{\partial^2\zeta_0}{\partial y^2} = q^2\zeta_0, \qquad \frac{d^2\zeta_1}{dx^2} = q^2\zeta_1 \tag{8.50}$$

The solution for $\zeta_1(x)$, which levels off at infinity, has the form:

$$\zeta_1(x) = q^{-1}\tan\psi_1 \exp(-qx) \qquad \text{(fixed contact angle } \alpha_1 = 90° - \psi_1) \tag{8.51}$$

$$\zeta_1(x) = H\exp(-qx) \qquad \text{(fixed contact line on the wall)} \tag{8.52}$$

On the other hand, $\zeta_0(x,y)$ corresponds to the configurations depicted in Fig. 8.10, and consequently, $\zeta_0(x,y)$ is determined by Eqs. (7.38)–(7.44) with $Q_1 = Q_2$ in the case of fixed contact angle and with $Q_1 = -Q_2$ in the case of fixed contact line. Further, in the case of fixed contact *angle* the shape of the contact line on the particle surface, $\zeta_0(\omega)$, is determined by Eq. (7.64), that is

$$\zeta_0(\omega) = h_{2\infty} + Q_2 K_0\left(\frac{2qa^2}{s - r_2\cos\omega}\right), \qquad \text{(fixed contact angle } \alpha_1) \tag{8.53}$$

In Eq. (8.53) ω is bipolar coordinate, cf. Eq. (7.25); in addition,

$$h_{2\infty} \approx Q_2 \ln\frac{2}{\gamma_e q r_2}\ , \qquad a = (s^2 - r_2^2)^{1/2}. \tag{8.54}$$

The validity of Eq. (8.53) is limited to small particles, $(qr_2)^2 << 1$, and small meniscus slope, $|\nabla_{II}\zeta_0|^2 << 1$, which is the case considered here.

Next, our purpose is to derive a counterpart of Eq. (8.53) for the case of fixed contact *line* at the wall. As in Section 7.2.2 we will use the method of the matched ("outer" and "inner") asymptotic expansions [13]. For large particle-wall separations, $(qa)^2 \geq 1$, one can use the superposition approximation representing the meniscus shape around a couple of particles (the particle and its mirror image) as a sum of the deformations, created by two isolated particles. Since the mirror image now has the opposite capillary charge (see Fig. 8.10b) the superposition approximation yields Eq. (7.59), but with "–" instead of "+" [9]:

$$\zeta_0^{\text{out}}(\omega) = Q_2 K_0(qr_r) - Q_2 K_0(qr_l), \qquad (qa)^2 \geq 1 \tag{8.55}$$

where the superscript "out" means that Eq. (8.55) is valid in the outer asymptotic region of not-too-small interparticle separations, $(qa)^2 \geq 1$, in which the superposition approximation can be applied; r_l and r_r are expressed again by Eq. (7.62). Taking into account the known asymptotic formula [14-16]

$$K_0(x) \approx \ln\frac{2}{\gamma_e x} \qquad \text{for } x << 1 \tag{8.56}$$

and using Eq. (7.62) one obtains the "inner" limit of Eq. (8.55) for $a \to 0$ (r_l, $r_r \to 0$):

$$(\zeta_0^{\text{out}})^{\text{in}} = Q_2 \ln(r_l/r_r) = Q_2 \ln[(a+s)/r_2] = Q_2 \tau_2 \tag{8.57}$$

Here τ_2 is the value of the bipolar coordinate τ at the contact line, see Eq. (7.57). On the other hand, analytical expression corresponding to the inner asymptotic region, $(qa)^2 << 1$, can be obtained setting $\tau = \tau_2$, $Q_1 = -Q_2$ and $\tau_1 = \tau_2$ in Eq. (7.42) [9]:

$$\zeta_0^{\text{in}}(\omega) = Q_2 \tilde{\tau}_2(\omega), \qquad (qa)^2 << 1, \tag{8.58}$$

where

$$\tilde{\tau}_2(\omega) \equiv \tau_2 + \sum_{n=1}^{\infty}\frac{2}{n}\tanh(n\tau_2)\exp(-n\tau_2)\cos(n\omega) \tag{8.59}$$

For large separations $\tau_2 \to \infty$, $\tilde{\tau}_2 \to \tau_2$, and then with the help of Eqs. (8.57) and (8.58) one may check that

$$(\zeta_0^{\text{in}})^{\text{out}} = (\zeta_0^{\text{out}})^{\text{in}}, \tag{8.60}$$

as required by the method of the matched asymptotic expansions [13]. Equation (8.58) can be represented in the equivalent form

$$\zeta_0^{\text{in}}(\omega) = Q_2 \ln\frac{2}{\gamma_e q r_2} - Q_2 \ln\frac{2}{\gamma_e q \tilde{r}_2(\omega)}, \qquad \tilde{r}_2(\omega) \equiv r_2 \exp\tilde{\tau}_2(\omega) \tag{8.61}$$

The compound solution, which is valid in both the "inner" and "outer" region reads [9]:

$$\zeta_0(\omega) = h_{2\infty} - \mathrm{K}_0(q\tilde{r}_2(\omega)) \qquad \text{(fixed contact line at the wall)} \tag{8.62}$$

where $h_{2\infty}$ is defined by Eq. (8.54) and $\tilde{r}_2(\omega)$ is defined by Eqs. (8.59) and (8.61). Having in mind Eq. (8.56) one sees that for small distances, $(qa)^2 << 1$, Eq. (8.62) reduces to the "inner" expression Eq. (8.61), whereas for longer distances, $(qa)^2 \geq 1$, Eq. (8.62) asymptotically tends to the "outer" expression Eq. (8.55).

Equations (8.53) and (8.62) will be used in Section 8.2.5 to quantify the particle–wall interaction in the framework of the force approach.

8.2.3. ELEVATION OF THE CONTACT LINE ON THE SURFACE OF THE FLOATING PARTICLE

Here we continue the theoretical description of the configurations of particle and wall depicted in Figs. 8.11 and 8.12. In Ref. [9] it has been established that the capillary charge of the floating particle is given by the expression

$$Q_2 = \tfrac{1}{2} q^2 [b_2^2 (R_2 - b_2/3) - \tfrac{4}{3} D_2 R_2^3 - r_2^2 h_2] \tag{8.63}$$

which is in fact Eq. (8.12) for $k = 2$, but the capillary elevation h_2 now has contributions from both the particle meniscus ζ_0 and the meniscus on the wall ζ_1, see Figs. 8.11 and 8.12, and Eq. (8.49):

$$h_2 = h_{20} + h_{21} \tag{8.64}$$

Below we specify the expressions for h_2 in the two alternative cases of fixed contact angle α_1 and fixed elevation H at the wall.

Fixed contact angle at the wall. As already discussed, in this case the shape of the meniscus ζ_0 is identical to that around two similar floating particles of capillary charge Q_2, see Fig. 8.10a. Consequently, h_{20} can be expressed by means of Eq. (7.55); in addition, h_{21} can be determined from Eq. (8.51): $h_{21} = \zeta_1(s)$. Thus in view of Eq. (8.64) one obtains [9]

$$h_2 = q^{-1} \tan\psi_1 \exp(-qs) + h_{2\infty} + Q_2 \mathrm{K}_0(q(s+a)) \qquad \text{(fixed contact angle } \alpha_1\text{);} \qquad (8.65)$$

see also Eq. (8.54).

Fixed contact line at the wall. In this case h_{21} can be determined from Eq. (8.52):

$$h_{21} = \zeta_1(s) = H\exp(-qs) \qquad (8.66)$$

To determine h_{20} we will employ again the method of the matched asymptotic expansions. The value of h_{20} in the inner asymptotic region of short particle-wall separations can be obtained by integration of Eqs. (8.58)–(8.59) in accordance with Eq. (7.47):

$$h_{20}^{\mathrm{in}} \equiv \frac{1}{2\pi r_2} \oint_{C_2} \zeta_0^{\mathrm{in}}\, dl = Q_2 \hat{\tau}_2 \qquad (qa)^2 << 1, \qquad (8.67)$$

where

$$\hat{\tau}_2 \equiv \tau_2 + \sum_{n=1}^{\infty} \frac{2}{n} \tanh(n\tau_2) \exp(-2n\tau_2), \qquad \tau_2 = \ln[(a+s)/r_2]. \qquad (8.68)$$

On the other hand, in the outer asymptotic region of longer particle-wall separations h_{20} can be expressed by means of Eq. (7.53) with $Q = -Q_2$:

$$h_{20}^{\mathrm{out}} = h_{2\infty} - Q_2 K_0(2qs) \qquad (qa)^2 \geq 1, \qquad (8.69)$$

Equation (8.67) can be rewritten in the form

$$h_{20}^{\mathrm{in}} = Q_2 \ln\frac{2}{\gamma_{\mathrm{e}} q r_2} - Q_2 \ln\frac{2}{\gamma_{\mathrm{e}} q r_2 \exp\hat{\tau}_2} \qquad (qa)^2 << 1 \qquad (8.70)$$

The compound expression can be formally obtained if the logarithms in Eq.(8.70) are exchanged with K_0-functions in agreement with Eq. (8.56) [9]:

$$h_{20} = h_{2\infty} - Q_2 K_0(qr_2 \exp\hat{\tau}_2) \tag{8.71}$$

see also Eq. (8.54). For short particle-wall separations Eq. (8.71) reduces to Eq. (8.70), whereas for longer separations $\hat{\tau}_2 \to \tau_2$ and Eq. (8.71) transforms into Eq. (8.69). Finally, substituting Eqs. (8.66) and (8.71) into Eq. (8.64) one obtains the sought-for expression for the capillary elevation of the contact line on the particle surface:

$$h_2 = H\exp(-qs) + h_{2\infty} - Q_2 K_0(qr_2 \exp\hat{\tau}_2) \qquad \text{(fixed elevation at the wall)} \tag{8.72}$$

8.2.4. ENERGY OF CAPILLARY INTERACTION

In accordance with Eq. (7.16) the energy and the force of capillary interaction can be presented in the form

$$\Delta\Omega = \Omega(s) - \Omega(\infty) = \Delta W_{\rm w} + \Delta W_{\rm m} + \Delta W_{\rm g}, \qquad F = -d(\Delta\Omega)/ds, \tag{8.73}$$

where the additive constant in the expression for $\Delta\Omega$ is determined in such a way that $\Delta\Omega \to 0$ for $s \to \infty$; the last three terms in the expression for $\Delta\Omega$ represent the wetting, meniscus and gravitational contributions, respectively. Following the derivation of Eq. (8.23) one can deduce [9]:

$$\Delta W_{\rm w} = -2\pi\sigma\,[R_2 b_2 \cos\alpha_2 + \lambda Q_2 q^{-1} \tan\psi_1 \exp(-qa)] - W_{\rm w\infty}, \tag{8.74}$$

where λ is defined by Eq. (8.47) and the constant $W_{\rm w\infty}$ is defined in such a way that $\Delta W_{\rm w} \to 0$ for $s \to \infty$; the two terms in the brackets represent, respectively, contributions from the wetting of the particle and the wall. Further, in Ref. [9] it is proven that the sum of the gravitational and the meniscus surface energy can be expressed in the form

$$\Delta W_{\rm m} + \Delta W_{\rm g} = \Delta\widetilde{W}_{\rm m} + \Delta\widetilde{W}_{\rm g} \tag{8.75}$$

where $\Delta\widetilde{W}_{\rm g}$ is defined by a counterpart of Eq. (8.28),

$$\Delta\widetilde{W}_{\rm g} = -\pi\sigma\left\{2Q_2 h_2 - q^2[\tfrac{1}{4}(r_2^2 - 2h_2^2)r_2^2 + (\tfrac{4}{3}D_2 R_2^3 - R_2 b_2^2 + \tfrac{1}{3}b_2^3)(R_2 - b_2)]\right\} - \widetilde{W}_{g\infty} \tag{8.76}$$

and

$$\Delta\widetilde{W}_{\rm m} = \pi\sigma\left[Q_2 h_2 - (-1)^{\lambda} Q_2 \zeta_1(s) - r_2^2 - \tfrac{1}{2}(qr_2)^2 \zeta_1^2(s)\right] - \Delta\widetilde{W}_{\rm m\infty} \tag{8.77}$$

Here λ is defined by Eq. (8.47); $\zeta_1(x)$ is to be calculated from Eq. (8.51) or (8.52) depending on whether the contact angle or contact line is fixed at the wall; likewise, h_2 is to be calculated from either Eq. (8.65) or Eq. (8.72); the constant $\Delta\widetilde{W}_{\mathrm{m}\infty}$ is defined in such a way that $\Delta\widetilde{W}_{\mathrm{m}} \to 0$ for $s \to \infty$. Equations (8.73)–(8.77) determine the dependence $\Delta\Omega = \Delta\Omega(s)$. A convenient procedure of numerical calculations is described in Section 8.2.6 below.

A relatively accurate and simple asymptotic formula for the force F experienced by the floating particle can be derived in the following way [9]. Equation (8.31) for $k = 2$ can be presented in the form:

$$\frac{db_2}{ds} = -r_2 \frac{d\psi_2}{ds} = \frac{r_2}{R_2 - b_2}\frac{dr_2}{ds} = -\frac{dQ_2}{ds}[1 + O(q^2 R_2^2)] = \tfrac{1}{2}(qr_2)^2 \frac{dh_2}{ds}[1 + O(q^2 R_2^2)], \quad (8.78)$$

see also Eq. (8A.3) in Appendix 8A. The differentiation of Eq. (8.74), along with Eqs. (8.77), gives:

$$\frac{d\Delta W_{\mathrm{w}}}{ds} = \pi\sigma\left[-(qr_2)^2 R_2 \cos\alpha_2 \frac{dh_2}{ds} + \lambda\left(2Q_2 + qr_2^2 \frac{dh_2}{ds}\right)\tan\psi_1 \mathrm{e}^{-qs}\right][1 + O(q^2 R_2^2)] \quad (8.79)$$

Next, differentiating Eq. (8.77) along with Eq. (8.78), and taking into account that $b_2 - R_2 \approx R_2\cos\alpha_2$ and $d\zeta_1(s)/ds = -q\zeta_1(s)$, see Eqs. (8.51)–(8.52), one obtains:

$$\begin{aligned}\frac{d\Delta\widetilde{W}_{\mathrm{m}}}{ds} = \pi\sigma\Big\{&\Big[Q_2 - \tfrac{1}{2}(qr_2)^2 h_2 + (qr_2)^2 R_2 \cos\alpha_2\Big]\frac{dh_2}{ds} + \\ &\left(Q_2 + \tfrac{1}{2}qr_2^2 \frac{dh_2}{ds}\right)(-1)^{\lambda} q\,\zeta_1(s) + q\big[qr_2\zeta_1(s)\big]^2\Big\} \times [1 + O(q^2 R_k^2)]\end{aligned} \quad (8.80)$$

The differentiation of Eq. (8.76) gives an expression analogous to Eq. (8.34):

$$\frac{d\Delta\widetilde{W}_{\mathrm{g}}}{ds} = -\pi\sigma \sum_{k=1,2} 2Q_2 \frac{dh_2}{ds}[1 + O(q^2 R_2^2)] \quad (8.81)$$

Since our purpose is to obtain the long distance asymptotics, that for $s >> r_2$, we notice that in this limit both Eq. (8.65) and Eq. (8.72) can be presented in the form

$$h_2 \approx \zeta_1(s) + h_{2\infty} + Q_2 \mathrm{K}_0(2qs), \qquad s >> r_2, \quad (8.82)$$

Then in view of Eqs. (8.51)–(8.52) one obtains

$$\frac{dh_2}{ds} \approx -q\zeta_1(s) - 2qQ_2\mathrm{K}_1(2qs), \qquad s >> r_2, \tag{8.83}$$

Finally, in accordance with Eq. (8.73) we sum up Eqs. (8.79)–(8.81) and substitute Eq. (8.83) in the result; after some algebra we obtain [9]:

$$F(s) \approx -\pi\sigma q\left[2Q_2\zeta_1(s) + \left(qr_2\zeta_1(s)\right)^2 - 2(-1)^{\lambda}Q_2^2\mathrm{K}_1\left(2qs\right)\right]\left(1 + O(q^2R_2^2)\right) \qquad (s >> r_2) \tag{8.84}$$

$\zeta_1(s)$ is to be substituted from Eq. (8.51) or (8.52) depending on the boundary condition on the wall; λ is defined by Eq. (8.47). The range of validity of Eq. (8.84) is verified in Fig. 8.15 below. The meaning of the three terms in Eq. (8.84) is the following.

First we notice that the gravitational force exerted on the particle is $F_g \approx 2\pi r_2\sigma\sin\psi_2 = 2\pi\sigma Q_2$, cf. Eq. (8.1). In addition, the slope of the interface is characterized by

$$\sin\psi(s) \approx \tan\psi(s) = d\zeta_1(s)/ds = -q\zeta_1(s). \tag{8.85}$$

Then one obtains $-2\pi\sigma\, Q_2\, q\zeta_1(s) = F_g \sin\psi(s)$. Hence, the first term in the brackets in Eq. (8.84) expresses the effect of the *gravitational force*, $F_g \sin\psi(s)$, which tends to "slide" the particle along the inclined meniscus.

The second term in the brackets in Eq. (8.84), $-\pi\sigma q(qr_2\zeta_1(s))^2$, is proportional to πr_2^2, that is to the area encircled by the contact line. This term takes into account the *pressure jump* across the interface. The respective force can be estimated multiplying the area πr_2^2 by the hydrostatic pressure $\Delta\rho g h_2$ and by $\sin\psi(s) \approx -q\zeta_1(s)$ to take a projection along the tangent to the meniscus. Taking into account the fact that $h_2 \approx \zeta_1(s)$ and $\Delta\rho g = \sigma q^2$, one obtains $(\pi r_2^2)(\Delta\rho g h_2)\sin\psi(s) = -\pi\sigma q(qr_2\zeta_1(s))^2$. This term is always negative, i.e. it always corresponds to an effective particle-wall attraction [9].

The third term in the brackets in Eq. (8.84), $2\pi\sigma(-1)^{\lambda}qQ_2^2\mathrm{K}_1\left(2qs\right)$, expresses the contribution of the capillary image force, see Eq. (8.37), which is attractive in the case of fixed contact angle at the wall (Fig. 8.10a), but repulsive in the case of fixed contact line at the wall (Fig. 8.10b).

Equation (8.84) has found applications for the interpretation of experimental data about the measurement of the surface drag coefficient of floating particles and surface shear viscosity of

surfactant adsorption monolayers, see Section 8.2.7 below. Note that Eq. (8.84) can be integrated at fixed Q_2 to obtain an approximate expression for the interaction energy [9]:

$$\Delta\Omega(s) \approx -\pi\sigma\left[2Q_2\,\zeta_1(s) + \frac{1}{2}\left(q\,r_2\,\zeta_1(s)\right)^2 - (-1)^{\lambda}\,Q_2^2\,\mathrm{K}_1(2q\,s)\right]\left(1 + O\left(q^2\,R_2^2\right)\right); \quad (s >> r_2) \quad (8.86)$$

The range of validity of Eq. (8.86) is verified in Fig. 8.14 below.

8.2.5. APPLICATION OF THE FORCE APPROACH TO QUANTIFY THE PARTICLE–WALL INTERACTION

General equations. Our purpose is to directly calculate the x-component of the force exerted on the floating particle in Figs. 8.11 and 8.12. In agreement with Eqs. (7.21)–(7.23) one obtains

$$F_x = F_x^{(\sigma)} + F_x^{(p)} \quad (8.87)$$

$$F_x^{(\sigma)} = \mathbf{e}_x \cdot \oint_{L_2} dl\ \underline{\boldsymbol{\sigma}}\,, \qquad F_x^{(p)} = \mathbf{e}_x \cdot \oint_{S_2} ds\,(-\mathbf{n}P)\,, \quad (8.88)$$

where $\underline{\boldsymbol{\sigma}}$ is the vector of surface tension, P is hydrostatic pressure, L_2 denotes the contact line on the particle surface S_2, the latter having a running unit normal $\mathbf{n}$; dl and ds are linear and surface elements. The gravitational force is directed along the z-axis, and consequently, it does not (directly) contribute to F_x (although it contributes indirectly to F_x through $F_x^{(\sigma)}$, see below). To calculate $F_x^{(p)}$ one can use Eq. (7.137), that is

$$F_x^{(p)} = \Delta\rho g r_2 \int_0^{\pi} \zeta^2(\varphi)\cos\varphi\, d\varphi \quad (8.89)$$

Note that in view of Eq. (8.49) $\zeta = \zeta_0 + \zeta_1$. Usually ζ_0 is expressed in terms of the bipolar coordinate ω: $\zeta_0 = \zeta_0(\omega)$. Then to carry out the integration in Eq. (8.89) one can use the following relationships between the azimuthal angle φ and ω [17]:

$$\cos\omega = \frac{s\cos\varphi + r_2}{s + r_2\cos\varphi}, \qquad \frac{d\omega}{d\varphi} = \frac{a}{s + r_2\cos\varphi} \quad (8.90)$$

where $0 \le \omega \le \pi$ and $0 \le \varphi \le \pi$.

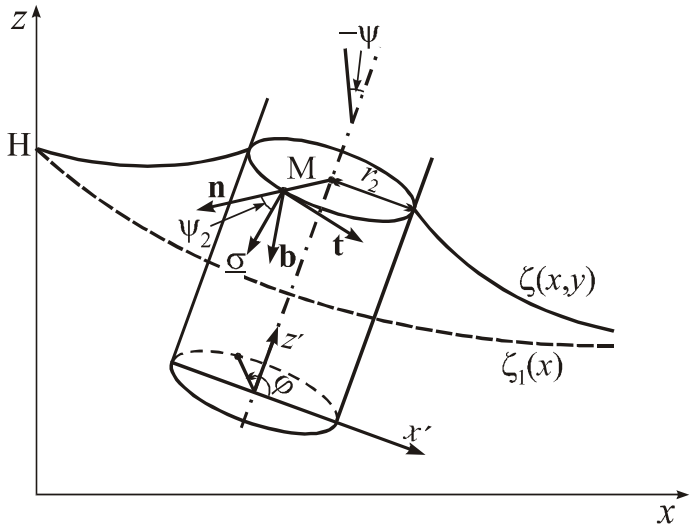

Fig. 8.13. Sketch of an auxiliary cylinder of radius r_2, whose generatrix is orthogonal to the surface $\zeta_1(x)$ of the non-disturbed meniscus at the wall and passes through the contact line on the particle surface. The angle between the running unit normal **n** to the surface of this cylinder and the vector of surface tension $\underline{\boldsymbol{\sigma}}$ is equal to ψ_2 in each point of the contact line; **t** is unit vector tangential to the contact line and $\mathbf{b} \equiv \mathbf{t} \times \mathbf{n}$.

Next, we continue with the calculation of the force $F_x^{(\sigma)}$ which is due to the vector of surface tension $\underline{\boldsymbol{\sigma}}$ integrated along the contact line. First, let us consider an auxiliary cylinder of radius r_2, whose generatrix is orthogonal to the surface $\zeta_1(x)$ and passes through the contact line on the particle surface, see Fig. 8.13. The angle between the running unit normal to the surface of this cylinder, **n**, and the surface tension vector $\underline{\boldsymbol{\sigma}}$ is equal to ψ_2 in each point of the contact line. Let us introduce a coordinate system (x', y', z'), whose z'-axis coincides with the axis of the cylinder in Fig. 8.13. The unit basis vectors of the new coordinate system are

$$\mathbf{e}'_x = \mathbf{e}_x \cos\psi + \mathbf{e}_z \sin\psi, \qquad \mathbf{e}'_y = \mathbf{e}_y, \qquad \mathbf{e}'_z = \mathbf{e}_z \cos\psi - \mathbf{e}_x \sin\psi. \tag{8.91}$$

where $\psi = \psi(s)$ is the local slope of the meniscus on the wall, see Eq. (8.85) and Fig. 8.13. The linear element dl along the contact line and its running unit tangent **t** are expressed as follows

$$dl = r_2 \chi \, d\varphi, \qquad \chi \equiv \left[1 + \left(\frac{1}{r_2} \frac{d\zeta_0}{d\varphi} \right)^2 \right]^{1/2} \tag{8.92}$$

$$\mathbf{t} = \frac{1}{\chi} \left[-\mathbf{e}'_x \sin\varphi + \mathbf{e}'_y \cos\varphi + \mathbf{e}'_z \frac{1}{r_2} \frac{d\zeta_0}{d\varphi} \right] \tag{8.93}$$

The running unit normal to the surface of the cylinder **n** and the running binormal **b** are defined as follows (Fig. 8.13):

$$\mathbf{n} = \mathbf{e}'_x \cos\varphi + \mathbf{e}'_y \sin\varphi, \qquad \mathbf{b} = \mathbf{t} \times \mathbf{n} \tag{8.94}$$

The vector of surface tension $\underline{\boldsymbol{\sigma}}$ belongs to the plane formed by the vectors **n** and **b**:

$$\underline{\boldsymbol{\sigma}} = \sigma(\mathbf{b}\sin\psi_2 + \mathbf{n}\cos\psi_2) \tag{8.95}$$

Combining Eqs. (8.91)–(8.95) one obtains:

$$\sigma_x \equiv \mathbf{e}_x \cdot \underline{\boldsymbol{\sigma}} = \sigma\left[\frac{1}{\chi}\sin\psi_2 \sin\psi + \left(-\frac{1}{r_2\chi}\frac{d\zeta_0}{d\varphi}\sin\psi_2 \sin\varphi + \cos\psi_2 \cos\varphi\right)\cos\psi\right] \tag{8.96}$$

Finally, we combine Eqs. (8.88) with Eqs. (8.92) and (8.96) to derive [9]

$$F_x^{(\sigma)} = \oint_{L_2} \sigma_x dl = 2\pi\sigma r_2 \sin\psi_2 \sin\psi - 2\sigma \sin\psi_2 \int_0^\pi \frac{d\zeta_0}{d\varphi}\sin\varphi d\varphi + \Delta F_x^{(\sigma)} \tag{8.97}$$

where

$$\Delta F_x^{(\sigma)} = 2\sigma r_2 \cos\psi_2 \cos\psi \int_0^\pi \chi \cos\varphi d\varphi \approx \frac{\sigma}{r_2}\int_0^\pi \left(\frac{d\zeta_0}{d\varphi}\right)^2 \cos\varphi d\varphi \tag{8.98}$$

In view of Eqs. (8.5), (8.85), (8.87), (8.89), (8.97) and (8.98) the net capillary force exerted on the floating particle in the vicinity of the wall is [9,18]

$$F \approx F_x = -2\pi\sigma Q_2 q \zeta_1(s) + (\sigma/r_2)\int_0^\pi [\,2Q_2\zeta_0(\varphi) + (d\zeta_0/d\varphi)^2 + q^2 r_2^2 \zeta^2]\cos\varphi\, d\varphi \tag{8.99}$$

Note that $\zeta = \zeta_0 + \zeta_1$; in the case of fixed contact *angle* ζ_1 and ζ_0 are given by Eqs. (8.51) and (8.53); in the case of fixed contact *line* ζ_1 and ζ_0 are given by Eqs. (8.52) and (8.62); to derive Eq. (8.99) we have used integration by parts in Eq. (8.97). The integral in Eq. (8.99) is to be taken numerically. In Ref. [18] Eq. (8.99) was applied to interpret experimental data for the equilibrium distance between floating particle and vertical wall, see Section 8.2.7 for details.

Asymptotic expression for long distances. For long distances ($s >> r_2$) the last two terms in Eq. (8.97) yield Eq. (7.145), where $L = 2s$ and $Q_1Q_2 = (-1)^\lambda Q_2^2$, see Eq. (8.47) and Fig. 8.10; then in view of Eq. (8.85) we obtain the respective asymptotic form of Eq. (8.97):

$$F_x^{(\sigma)} = -2\pi\sigma[Q_2 q\zeta_1(s) - (-1)^{\lambda} q Q_2^2 \mathrm{K}_1(2qs)] \qquad (s >> r_2) \qquad (8.100)$$

For not extremely small angle ψ_1 and not-too-large capillary charge Q_2 one can estimate $F_x^{(p)}$ using the following approximation for the shape of the contact line:

$$\zeta(\varphi) \approx \zeta_1(s) + \left.\frac{d\zeta_1}{dx}\right|_{x=s} r_2 \cos\varphi \qquad (8.101)$$

The substitution of Eq. (8.101) into Eq. (8.89), in view of Eq. (8.85), yields

$$F_x^{(p)} \approx \pi\sigma(qr_2)^2[\zeta_1(d\zeta_1/dx)]_{x=s} = -\pi\sigma q[qr_2\zeta_1(s)]^2, \qquad (s >> r_2,\ \sin^2\psi << 1) \quad (8.102)$$

Since $F \approx F_x = F_x^{(\sigma)} + F_x^{(p)}$, one sums up Eqs. (8.100) and (8.102) and as a result one arrives again at Eq. (8.84). In other words the energy and the force approaches give the same asymptotic expression for the capillary force, as it should be expected.

8.2.6. NUMERICAL PREDICTIONS OF THE THEORY AND DISCUSSION

The procedure of numerical calculations, proposed in Ref. [9], is the following:

(i) The input parameters are the mass densities of the phases, ρ_1, ρ_{II} and ρ_2, the particle radius and contact angle, R_2 and α_2, and the distance s between the particle and wall. Then $q = (\Delta\rho g/\sigma)^{1/2}$ and from Eq. (8.11) one calculates D_2. In addition, the parameters ψ_1 and H are known in the case of fixed contact angle or line, respectively, see Fig. 8.10. Note that ψ_1 and H can be both positive and negative; for example, in Fig. 8.11 ψ_1 is positive, whereas in Fig 8.12 H is negative.

(ii) Equations (8.5), (8.63), (8.65) and the two geometrical relationships,

$$b_2 = R_2[1 + \cos(\alpha_2 + \psi_2)], \qquad r_2 = [(2R_2 - b_2)b_2]^{1/2} \qquad (8.103)$$

form a set of five equations for determining the five unknown variables Q_2, ψ_2, h_2, r_2 and b_2. Note that Eq. (8.72) must be used instead of Eq. (8.65) when the contact line (rather than the contact angle) is fixed at the wall. To solve the aforementioned system of five equations one may use the following procedure of iterations [9]:

(1) As a zeroth-order approximation one may use $r_2^{(0)} = R_2 \sin\alpha_2$, $\psi_2^{(0)} = 0$ and $Q_2^{(0)} = 0$;

(2) $Q_2^{(k+1)} = r_2^{(k)} \sin\psi_2^{(k)}$, $k = 0, 1, 2,...$; cf. Eq. (8.5);

(3) $h_2^{(k+1)}$ is calculated from the values of $r_2^{(k)}$ and $Q_2^{(k)}$: in the case of fixed contact *angle* Eq. (8.65) is used; in the case of fixed contact *line* Eq. (8.72) is used;

(4) $b_2^{(k+1)}$ and $r_2^{(k+1)}$ are calculated from the value of $\psi_2^{(k)}$ using Eq. (8.103);

(5) $\psi_2^{(k+1)}$ is calculated from Eq. (8.63), along with Eq. (8.5), substituting the values of $h_2^{(k)}$, $b_2^{(k)}$ and $r_2^{(k)}$;

(6) If $|1 - Q_2^{(k)}/Q_2^{(k+1)}| < \varepsilon$ the iteration process stops; otherwise the iterations continue from step (2). Here ε is a small parameter determining the accuracy of the numerical calculations; for example, one could set $\varepsilon = 10^{-8}$.

(iii) The limiting (for $s\to\infty$) values $Q_{2\infty}$, $\psi_{2\infty}$, $h_{2\infty}$, $r_{2\infty}$ and $b_{2\infty}$ are determined from the same set of five equations, in which Eq. (8.65) or (8.72) for h_2 is exchanged with Eq. (8.54) for $h_{2\infty}$.

(iv) Using Eq. (8.73), along with Eqs. (8.74)–(8.77) one calculates the energy $\Delta\Omega$ and force F of capillary interaction by means of the *energy* approach.

(v) Alternatively, one can use the *force* approach, i.e. Eq. (8.99) along with Eqs. (8.51) and (8.53) in case of fixed contact *angle*, or along with Eqs. (8.52) and (8.62) in case of fixed contact *line*; thus the force F can be calculated for each given distance s, and then the energy $\Delta\Omega$ can be obtained by means of numerical integration of the function $F(s)$.

In Ref. [9] it was established that the numerical procedures based on the energy and force approaches give very close results; small differences may originate from the used approximations for small particle and small meniscus slope.

Numerical results and discussion. As illustrative examples here we present numerical results obtained in Ref. [9]. The curves in Figs. 8.14a and 8.14b are calculated for the same particle (R_2 = 500 μm, α_2 = 70°) floating at air-water interface (σ = 72.4 mN/m, $\Delta\rho$ = 1.0 g/cm^3), but the boundary conditions at the wall are different: fixed contact *angle* $\alpha_1 = 90° - \psi_1$ (Fig. 8.14a) and fixed contact *line* (Fig. 8.14b). The solid lines are calculated using the procedure described above, whereas the dashed lines are obtained by means of the approximate expression Eq. (8.86), where $\zeta_1(s)$ is determined from Eqs. (8.51) or (8.52). One sees that the

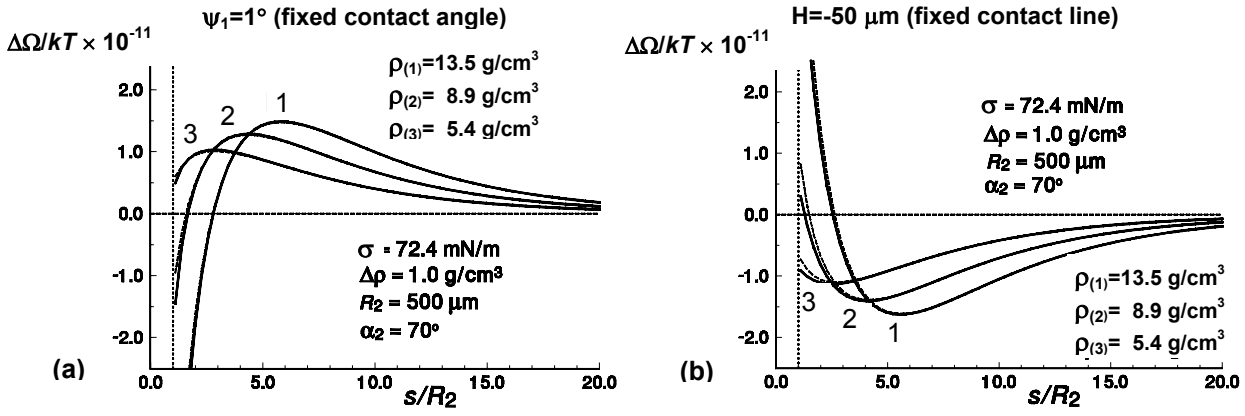

Fig. 8.14. Plots of the interaction energy $\Delta\Omega$ vs. separation s between a floating particle and a wall: (a) in the case of fixed contact angle at the wall ($\alpha_1 = 90° - \psi_1 = \text{const.}$) and (b) in the case of fixed contact line at the wall ($H = \text{const}$). The different curves, calculated in Ref. [9], correspond to different values of particle mass density. The solid and dashed lines are obtained using Eqs. (8.73) and (8.86) respectively.

approximate expression (8.86) is rather accurate, except for very short particle-wall separations. The different curves in Fig. 8.14, as well as in Fig. 8.15, are calculated for three different values of the particle mass density, corresponding to the densities of mercury, copper and titanium. The most important difference between the curves in Fig. 8.14a and 8.14b is that a *maximum* of $\Delta\Omega$ (state of unstable equilibrium) exists in the case of fixed contact angle (cf. Fig. 8.11), whereas a *minimum* of $\Delta\Omega$ (state of stable equilibrium) is present in the case of fixed contact line (cf. Fig. 8.12). The existence of such a state of stable equilibrium at some distance $s = s^*$ has been established experimentally in Ref. [18], see Section 8.2.7 below.

Figure 8.15 shows the curves of the force F vs. distance s, corresponding to the curves $\Delta\Omega$ vs. s in Fig. 8.14. The solid lines are calculated by means of the more rigorous set of equations, Eqs. (8.73)–(8.77), whereas the dashed lines are obtained by means of the approximate Eq. (8.84). One sees that the latter approximate formula gives amazingly good numerical results. Qualitatively the plots of F vs. s in Fig. 8.15 look similar to the plots of $\Delta\Omega$ vs. s in Fig. 8.14; the points in which $F = 0$ correspond to the maxima or minima of the $\Delta\Omega(s)$ curves. In the latter points the capillary image force, that is the term

$$F_{\text{image}} \equiv 2\pi\sigma(-1)^{\lambda} q Q_2^{\,2}\, \mathrm{K}_1(2qs) \tag{8.104}$$

in Eq. (8.84) is exactly counterbalanced by the gravitational force exerted on the particle

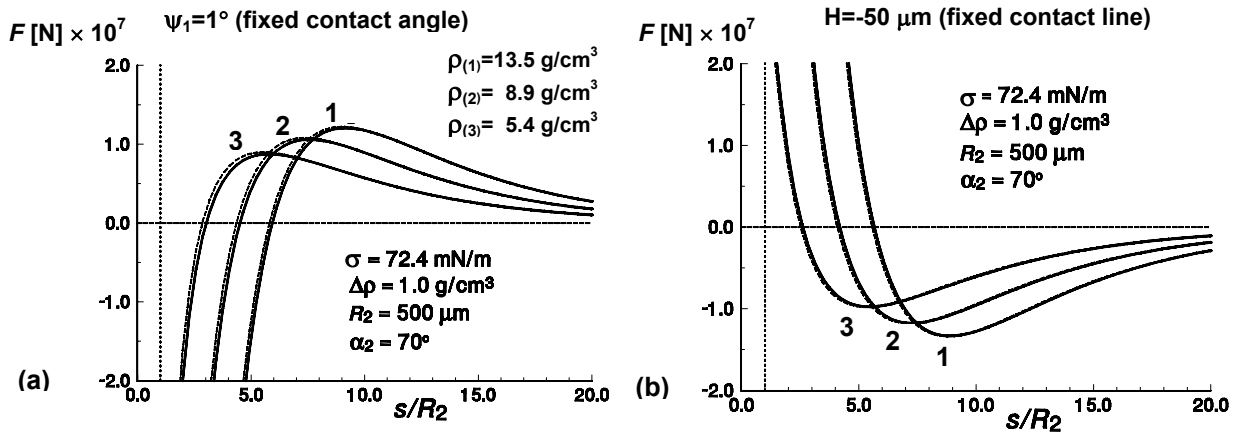

Fig. 8.15. Plots of the interaction force F vs. separation s between a floating particle and a wall: (a) in the case of fixed contact angle at the wall ($\alpha_1 = 90° - \psi_1 = \text{const.}$) and (b) in the case of fixed contact line at the wall ($H = \text{const}$). The different curves, calculated in Ref. [9], correspond to different values of particle mass density. The solid and dashed lines are obtained using Eqs. (8.73) and (8.84) respectively.

(weight + buoyancy force), this is the term

$$F_{\text{gravity}} \equiv -\pi\sigma q[2Q_2\zeta_1(s) + (qr_2\zeta_1(s))^2] \tag{8.105}$$

in Eq. (8.84), i.e. $F = F_{\text{image}} + F_{\text{gravity}} = 0$.

It should be noted that the plot of F vs. s is not always non-monotonic as it is in Fig. 8.15. Indeed, if the contact angle α_1 in Fig. 8.11 were larger than 90°, or the contact line elevation H in Fig. 8.12 were positive, then F_{image} and F_{gravity} would have the same sign and the net dependence $F(s)$ would be monotonic.

To examine the dependence of the force F on the particle contact angle α_2 in Fig. 8.16 we plot the dependence of F vs. α_2 for a fixed particle-wall separation: $s = 5R_2$; the other parameter values are the same as in Figs 8.14 and 8.15. One sees that the dependence of F vs. α_2 is rather weak in both cases: fixed contact *angle* (Fig. 8.16a) and fixed contact *line* (Fig. 8.16b). This fact implies that measurements of the capillary force, F, or of the equilibrium distance particle-wall, s^*, cannot be used as a method for determining contact angles of small particles. On the other hand, it turns out that the theoretical results for F give the possibility to determine the drag coefficient of particles sliding down an inclined meniscus and then to extract the coefficient of surface shear viscosity from the data, see Section 8.2.7.

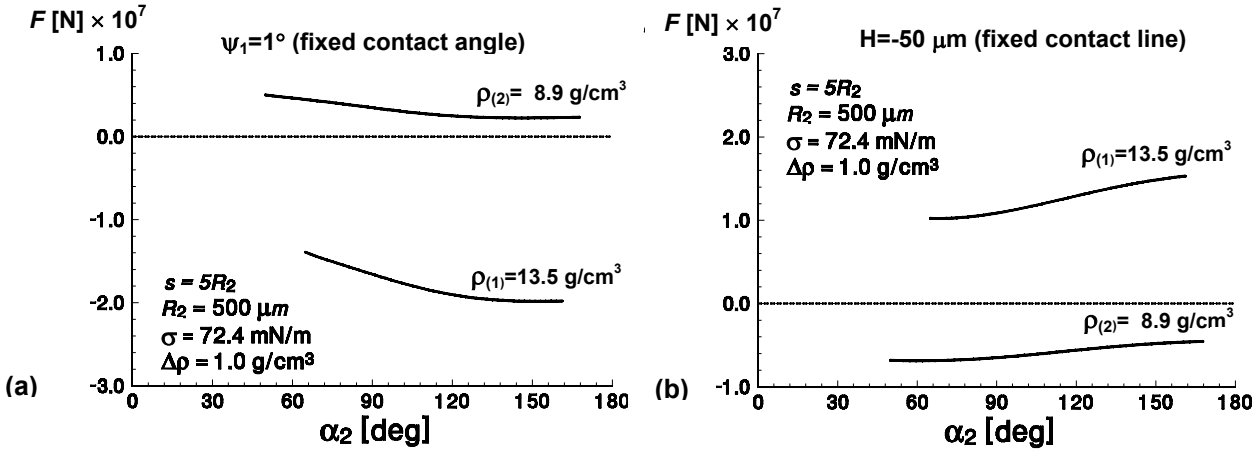

Fig. 8.16. Capillary force F as a function of the particle contact angle α_2 for a fixed value of the particle-wall separation, $s = 5R_2$: (a) in the case of fixed contact angle at the wall ($\alpha_1 = 90° - \psi_1$ = const.) and (b) in the case of fixed contact line at the wall (H = const). The two curves, calculated in Ref. [9], correspond to particle mass density $\rho_{(1)} = 13.5$ g/cm^3 and $\rho_{(2)} = 8.9$ g/cm^3.

8.2.7. EXPERIMENTAL MEASUREMENTS WITH FLOATING PARTICLES

The configuration with repulsive capillary image force, which is depicted in Fig. 8.12, is realized experimentally in Refs. [18] and [19] as shown in Fig. 8.17. In these experiments the "wall" is a hydrophobic Teflon barrier, whose position along the vertical can be precisely varied and adjusted. The total lateral capillary force exerted on the particle depicted in Fig. 8.17 can be described by the asymptotic expression Eq. (8.84) in which $\zeta_1(s)$ is substituted from Eq. (8.52):

$$F(s) \approx -\pi\sigma q\left[2Q_2 He^{-qs} + \left(r_2 qHe^{-qs}\right)^2 - 2Q_2^2 \mathrm{K}_1(2qs)\right]\left(1 + O(q^2 R_2^2)\right) \tag{8.106}$$

As before, H characterizes the position of the contact line on the wall with respect to the non-disturbed horizontal liquid surface far from the vertical plate (Fig. 8.17) and s is the particle-wall distance.

Equilibrium measurements. In keeping with the sign-convention accepted in the present chapter, both H and Q_2 in Eq. (8.106) should be negative quantities. Then the first two terms in the brackets in Eq. (8.106) are positive, whereas the third one is negative. Therefore, as

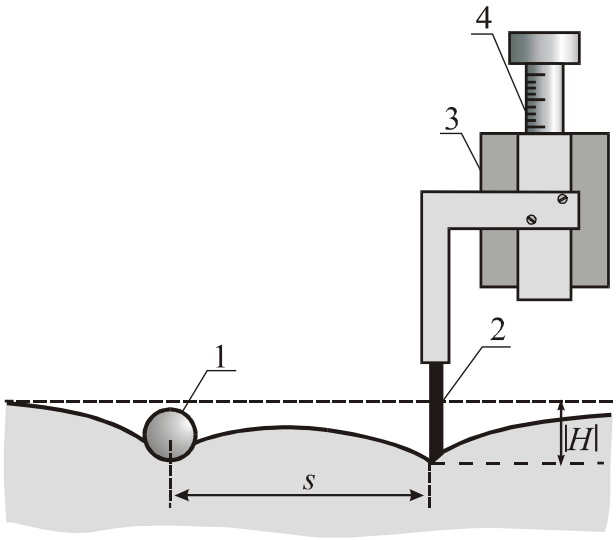

Fig. 8.17. Experimental set up for studying capillary interactions [18], for measurement of surface drag coefficient [19], and surface shear viscosity of surfactant adsorption monolayers [23]. Particle 1 is floating at a distance s from a hydrophobic plate 2, whose lower edge is located at a distance H below the level of the non-disturbed horizontal liquid surface; H can be varied by means of the micrometric table 3 and screw 4.

discussed in the previous section, for each given H there will be a distance $s = s^*$, corresponding to an equilibrium position of the particle, for which $F(s^*) = 0$. In other words, one can expect that a particle floating in a vicinity of the vertical wall (Fig. 8.17) will stay at an equilibrium distance s^* from the wall. The measurements carried out in Ref. [18] show that really this is the experimental situation. Varying H one can change the distance s^*. Figure 8.18 shows experimental points for H vs. s^* measured with a hydrophobized copper bead floating on the surface of pure water. The radius of the bead is $R_2 = 700 \pm 15$ μm and its contact angle with pure water is $\alpha_2 = 100°$. The accuracy and the reproducibility of the measurement are about ±2 μm for H and ±20 μm for s^*. The theoretical curve (the dashed line in Fig. 8.18) is drawn with $R_2 = 711$ μm which agrees well with the optically measured radius of the bead; the more rigorous expression Eq. (8.99) is used in the calculations, instead of the asymptotic formula Eq. (8.106). One sees in Fig. 8.18 that the agreement between theory and experiment is very good.

Figure 8.19 shows similar data as Fig. 8.18, however this time the floating particle is a mercury (Hg) drop. Since the mercury is liquid, the shape of the Hg drop is composed of two spherical

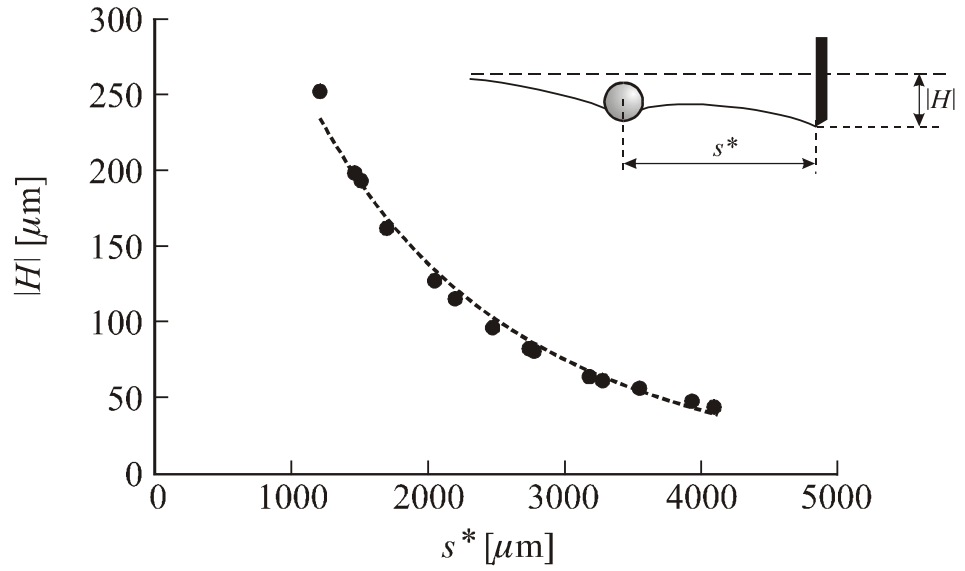

Fig. 8.18. Experimental data (•) from Ref. [18] for the dependence of H on s^* for a hydrophobized copper sphere, see the text for the notation. The line represents the theoretical dependence calculated by setting $F = 0$ in Eq. (8.99); experimental values of the contact angle $\alpha_2 = 100°$ and sphere radius $R_2 = 711$ μm are used.

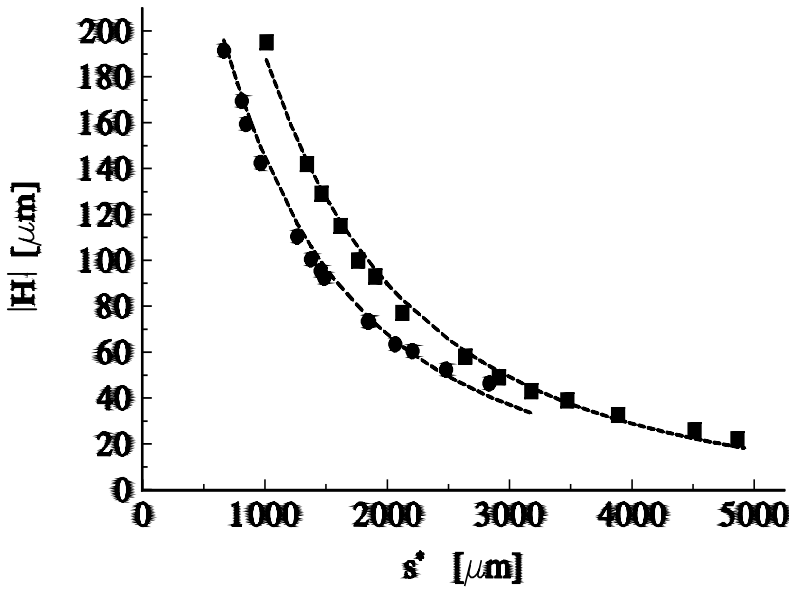

Fig. 8.19. Experimental data from Ref. [18] for the dependence of H on s^* for two mercury drops of different size. The lines represent theoretical fits calculated by means of Eq. (8.99) using the experimental values of the radii $R_w = 440$ μm (the lower curve) and $R_w = 512$ μm (the upper curve); the three-phase contact angle mercury-water-air is $\alpha_2 = 86°$.

segments of radii R_w and R_a, corresponding to the Hg-water and Hg-air regions. The values of R_w, R_a and of the contact angle α_2 have been determined in Ref. [18] by means of optical measurements. Then the theoretical plot of H vs. s^* has been calculated using Eq. (8.99) (see the dashed lines in Fig. 8.19) and compared with the experimental data (the symbols in Fig. 8.19). Again, there is an excellent agreement between theory and experiment. It should be noted that with the exception of an unknown (instrumental) additive constant in the experimental data for H, the theoretical curves in Fig. 8.19 are drawn without using any other adjustable parameter [18].

Dynamic measurements. It was demonstrated in Ref. [19] that if the capillary force F is calculated by means of Eq. (8.106), and the particle velocity, $\dot{s}$, is measured in dynamic experiments, then one can determine the drag force, F_d:

$$F_d = F - m\ddot{s}, \qquad F_d \equiv 6\pi\eta R_2 f_d \dot{s} \tag{8.107}$$

where R_2, m and $\ddot{s}$ are the particle radius, mass and acceleration, η is the viscosity of the liquid and f_d is the drag coefficient. If the particle were entirely immersed in the bulk liquid, F_d would

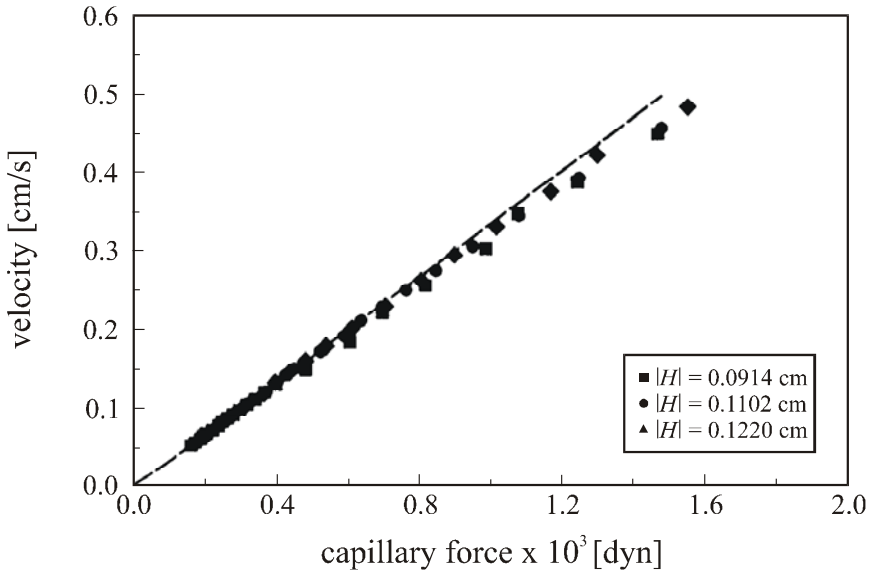

Fig. 8.20. Experimental data from Ref. [19] for the velocity $\dot{s}$ of a "sliding" glass sphere (Fig. 8.17) plotted vs. the capillary force F calculated from Eq. (8.106); the sphere is floating on the surface of pure water. The slope of the dashed line, drawn in accordance with Eq. (8.107) (the inertial term $m\ddot{s}$ neglected), gives drag coefficient f_d = 0.68. The data are obtained in 3 runs corresponding to 3 fixed values of H denoted in the figure.

be given by the Stokes formula, $F_d = 6\pi\eta R_2 \dot{s}$, and f_d would be equal to 1. In the considered case, f_d differs from unity because the particle is attached to the interface and protrudes from the underlying liquid phase. In Fig. 8.20 the experimentally measured velocity $\dot{s}$ of a particle approaching the wall is plotted vs. the capillary force $F(s)$, calculated by means of Eq. (8.106) for the experimental values of the distance s. The particle is a glass sphere of radius R_2 = 229 μm and contact angle α_2 = 48.7° at the surface of pure water, σ = 72 mN/m. The straight line in Fig. 8.20 corresponds to $F_d = F(s)$, i.e. drag force equal to the capillary force; from the slope of the straight line one determines f_d = 0.68. The slight deviation of the data from the straight line for the largest $F(s)$ is not a discrepancy between theory and experiment: this deviation is due to the inertia term $m\ddot{s}$ in Eq. (8.107), which is not negligible for shorter particle–wall distances, for which the approximation $F_d \approx F(s)$ is not good enough.

The hydrodynamic theory by Brenner and Leal [20,21], and Danov et al. [22], predicts that the drag coefficient f_d of a particle attached to a planar fluid interface is a function only of the of the viscosities of the two fluids and of the three-phase contact angle, α_2. The experiments in

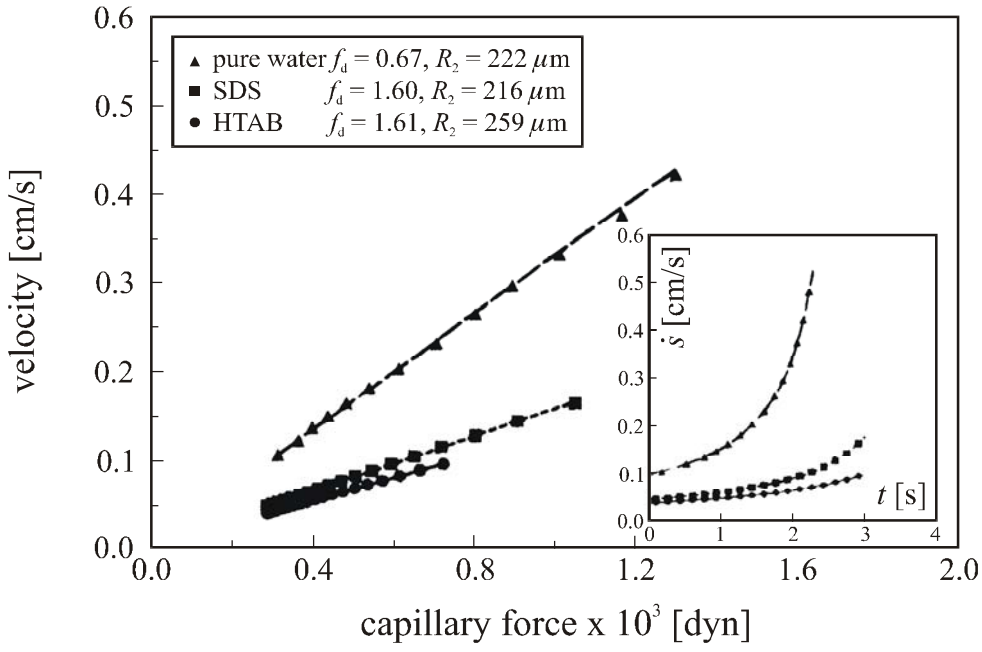

Fig. 8.21. Experimental data from Ref. [23] for the velocity $\dot{s}$ of a glass sphere plotted vs. the capillary force F calculated from Eq. (8.106). The slope of each experimental line gives the value of the drag coefficient, f_d . Data about the type of the solution, the determined f_d and the particle radius R_2 are given in the figure. The inset shows the experimental plot of $\dot{s}$ vs. time, which becomes linear if plotted as $\dot{s}$ vs. F.

Ref. [19] with particles on air–water interface give f_d varying between 0.68 and 0.54 for particle contact angle α_2 varying from 49° to 82° (the less the depth of particle immersion, the less the drag coefficient f_d); these experimentally obtained data for f_d are in a very good quantitative agreement with the hydrodynamic theory of the drag coefficient [22].

If the floating particle is heavy enough, it creates a considerable deformation of the surrounding liquid surface; this deformation travels together with the particle thus increasing f_d several times [19]; for the time being there is no quantitative hydrodynamic theory of the latter effect.

The addition of surfactant in the solution strongly increases f_d. The latter effect has been used in Ref. [23] to measure the surface viscosity of adsorption monolayers from low molecular weight surfactants exhibiting fast kinetics of adsorption. For these surfactants the surface viscosity is too low to be accessible to the conventional experimental methods, like the *deep-channel* surface viscometer [24-30], or the *disk* viscometer [31-37]. Fortunately, the motion of a sphere of radius 200–300 μm along a slightly inclined meniscus turns out to be sensitive to the friction within the adsorption layer (thick no more than 2 nm) of surfactants such as sodium dodecyl sulfate (SDS) and hexadecyl-trimethyl-ammonium-bromide (HTAB). This fact is utilized by the *sliding–particle* method for measurement of surface viscosity, which has been proposed in Ref. [23]. In Fig. 8.21 we present experimental data from Ref. [23] for the velocity $\dot{s}$ of a particle (Fig. 8.17) plotted vs. the capillary force $F(s)$, calculated by means of Eq. (8.106). One sees in Fig. 8.21 that again the data for $\dot{s}$ vs. $F(s)$ comply with straight lines, whereas the plots of $\dot{s}$ vs. time t are non-linear (see the inset in Fig. 8.21). From the slopes of the straight lines in Fig. 8.21 the drag coefficient f_d has been determined; the obtained values of f_d are also shown in Fig. 8.21. Note, that the addition of surfactant increases f_d from 0.66 (for pure water) up to 1.6. This effect, converted in terms of surface viscosity, gives respectively $\eta_s = 1.5$ and 2.0×10^{-6} kg/s for the surface viscosity of dense SDS and HTAB adsorption monolayers [23]. These results compare well with values of η_s obtained by means of *knife-edge* surface viscometers [38-43].

If the kinetics of surfactant adsorption is not fast enough to damp the surface elastic effects, the drag coefficient f_d can be influenced not only by the surface viscosity, but also by the surface

(Gibbs) elasticity (see Chapter 1 about the definitions of and theoretical expressions for the Gibbs elasticity and adsorption relaxation times). The complete theoretical dynamic problem, involving the effects of surface viscosity, surface elasticity and dynamics of surfactant adsorption has not yet been solved.

8.3. SUMMARY

In this chapter we presented theoretical and experimental results about the lateral capillary interaction between two floating particles, and between a floating particle and a vertical wall. The origin of this "flotation" force, F, is the overlap of the interfacial deformations created by the separate floating particles. In this aspect the "floatation" force is similar to the "immersion" force (see Chapter 7) and it is described by the same asymptotic formula, Eq. (8.4). The difference between the "flotation" and "immersion" forces is manifested through the different physical origin of the respective "capillary charge" Q, which results in a different dependence of Q on the interfacial tension σ and particle radius R. Thus in the case of "flotation" force $F \propto R^6/\sigma$, whereas in the case of "immersion" force $F \propto R^2\sigma$, see Eq. (8.20). The strong decrease of the "flotation" force with the diminishing of particle radius R leads to the consequence that this force becomes negligibly small for $R < 5$ μm, i.e. for Brownian particles, for which the "immersion" force is still rather powerful, see Fig. 8.3. In some aspect these two kinds of capillary interactions resemble the electrostatic and gravitational forces, which obey the same power law, but differ in the physical meaning and magnitude of the force constants (charges, masses).

The capillary charge of a floating particle can be calculated by means of Eq. (8.12) or by means of the more convenient, but approximate, Eq. (8.16). The energy of capillary interaction between floating particles is composed of contributions from the gravitational potential energy of particles and fluid phases, from the wetting of the particle surface and from the deformation of the fluid interface caused by the particles, see Eq. (8.26). In the asymptotic case of small deformations and long interparticle separations the sum of the aforementioned three contributions turns out to be equal to the half of the particle gravitational potential energy, see Eqs. (8.32)–(8.34); the latter finding validates the usage of the popular superposition approximation, Section 8.1.1. A convenient numerical procedure for a precise calculation of

the lateral flotation force is described, Section 8.1.5. Numerical data about the dependence of the interaction energy $\Delta\Omega$ on the interparticle distance L, particle radius R_k, density ρ_k and contact angle α_k, are presented and discussed. In all cases the capillary interaction between floating particles, as a function of L, is a *monotonic* attraction or repulsion depending on the sign of the product of the capillary charges: $Q_1Q_2 > 0$ or $Q_1Q_2 < 0$, see Figs. 8.5–8.9.

Next, we considered the case of a single particle floating in a vicinity of a vertical wall. Such a particle experiences the action of a capillary image force. The latter can be formally considered as interaction between the particle and its mirror image (with respect to the wall), which can be attraction or repulsion depending on whether the contact angle (Fig. 8.10a) or contact line (Fig. 8.10b) is fixed at the wall. If an inclined meniscus is formed in a neighborhood of the wall, then the interplay of the gravitational and capillary image forces can lead to a *non-monotonic* dependence of the interaction energy on the particle-wall distance, see Figs. 8.11, 8.12, 8.14 and 8.15. Analytical expressions for calculating the flotation interaction are obtained by means of both energy and force approaches, see Sections 8.2.4 and 8.2.5. A convenient asymptotic formula, Eq. (8.84), for the capillary force is obtained, which compares very well with the output of the more accurate theory, see Figs. 8.14 and 8.15. The derived expressions are in a very good agreement with experimental data for the equilibrium position of floating particles, Figs. 8.18 and 8.19. The obtained theoretical results have been applied to determine experimentally the drag coefficient of floating particles and the surface shear viscosity of surfactant adsorption monolayers, see Figs. 8.20 and 8.21.

Finally, we should note that in this chapter our attention was focused on the capillary interactions of floating *spherical* particles. In Refs. [44-47] one can find theoretical expressions and numerical results for two floating parallel horizontal *cylinders*.

8.4. REFERENCES

1. M.M. Nicolson, Proc. Cambridge Philos. Soc. 45 (1949) 288.
2. I.B. Ivanov, P.A. Kralchevsky, A.D. Nikolov, J. Colloid Interface Sci. 112 (1986) 97.
3. D.Y.C. Chan, J.D. Henry, L.R. White, J. Colloid Interface Sci. 79 (1981) 410.
4. V.N. Paunov, P.A. Kralchevsky, N.D. Denkov, K. Nagayama, J. Colloid Interface Sci. 157 (1993) 100.

5. E.D. Shchukin, A.V. Pertsov, E.A. Amelina, Colloid Chemistry, Moscow Univ. Press, Moscow, 1982 [in Russian].
6. P.A. Kralchevsky, K. Nagayama, Langmuir 10 (1994) 23.
7. P.A. Kralchevsky, K.D. Danov, N.D. Denkov, Chemical Physics of Colloid Systems and Interfaces, in: K.S. Birdi (Ed.) Handbook of Surface and Colloid Chemistry, CRC Press, Boca Raton, 1997.
8. P.A. Kralchevsky, K. Nagayama, Adv. Colloid Interface Sci. 85 (2000) 145.
9. P.A. Kralchevsky, V.N. Paunov, N.D. Denkov, K. Nagayama, J. Colloid Interface Sci. 167 (1994) 47.
10. P.A. Kralchevsky, N.D. Denkov, V.N. Paunov, O.D. Velev, I.B. Ivanov, H. Yoshimura, K. Nagayama, J. Phys.: Condens. Matter 6 (1994) A395.
11. L.D. Landau, E.M. Lifshitz, Electrodynamics of Continuous Media, Pergamon Press, Oxford, 1984.
12. J.N. Israelachvili, Intermolecular and Surface Forces, Academic Press, London, 1992.
13. A.H. Nayfeh, Perturbation Methods, Wiley, New York, 1973.
14. E. Janke, F. Emde, F. Lösch, Tables of Higher Functions, McGraw-Hill, New York, 1960.
15. H.B. Dwight, Tables of Integrals and Other Mathematical Data, Macmillan Co., New York, 1961.
16. M. Abramowitz, I.A. Stegun, Handbook of Mathematical Functions, Dover, New York, 1965.
17. V.N. Paunov, P.A. Kralchevsky, N.D. Denkov, I.B. Ivanov, K. Nagayama, Colloids Surf. 67 (1992) 138.
18. O.D. Velev, N.D. Denkov, P.A. Kralchevsky, V.N. Paunov, K. Nagayama, J. Colloid Interface Sci. 167 (1994) 66.
19. J.T. Petkov, N.D. Denkov, K.D. Danov, O.D. Velev, R. Aust, F. Durst, J. Colloid Interface Sci. 172 (1995) 147.
20. H. Brenner, L.G. Leal, J. Colloid Interface Sci. 65 (1978) 191.
21. H. Brenner, L.G. Leal, J. Colloid Interface Sci. 88 (1982) 136.
22. K.D. Danov, R. Aust, F. Durst, U. Lange, J. Colloid Interface Sci. 175 (1995) 36.
23. J.T. Petkov, K.D. Danov, N.D. Denkov, R. Aust, F. Durst, Langmuir 12 (1996) 2650.
24. W.D. Harkins, R. J. Meyers, Nature 140 (1937) 465.
25. D.G. Dervichian, M. Joly, J. Phys. Radium 10 (1939) 375.
26. J.T. Davies, Proc. 2nd Int. Congr. Surf. Act. 1 (1957) 220.
27. R.J. Mannheimer, R.S. Schechter, J. Colloid Interface Sci. 32 (1970) 195.

28. A.J. Pintar, A.B. Israel, D.T. Wasan, J. Colloid Interface Sci. 37 (1971) 52.
29. D.T. Wasan, V. Mohan, Interfacial rheological properties of fluid interfaces containing surfactants, in: D.O. Shah and R.S. Schechter (Eds.) Improved Oil Recovery by Surfactant and Polymer Flooding, Academic Press, New York, 1977, p. 161.
30. D.A. Edwards, H. Brenner, D.T. Wasan, Interfacial Transport Processes and Rheology, Butterworth-Heinemann, Boston, 1991.
31. F.C. Goodrich, A.K. Chatterjee, J. Colloid Interface Sci. 34 (1970) 36.
32. P.B. Briley, A.R. Deemer, J.C. Slattery, J. Colloid Interface Sci. 56 (1976) 1.
33. R. Shail, J. Engng. Math. 12 (1978) 59.
34. S.G. Oh, J.C. Slattery, J. Colloid Interface Sci. 67 (1978) 516.
35. A.M. Davis, M.E. O'Neill, Int. J. Multiphase Flow 5 (1979) 413.
36. R. Shail, D.K. Gooden, Int. J. Multiphase Flow 7 (1981) 245.
37. R. Miller, R. Wustneck, J. Krägel, G. Kretzschmar, Colloids Surf. A 111 (1996) 75.
38. A.G. Brown, W.C. Thuman, J.W. McBain, J. Colloid Sci. 8 (1953) 491.
39. N. Lifshutz, M.G. Hedge, J.C. Slattery, J. Colloid Interface Sci. 37 (1971) 73.
40. F.C. Goodrich, L.H. Allen, J. Colloid Interface Sci. 40 (1972) 329.
41. F.C. Goodrich, L.H. Allen, A.M. Poskanzer, J. Colloid Interface Sci. 52 (1975) 201.
42. A.M. Poskanzer, F.C. Goodrich, J. Colloid Interface Sci. 52 (1975) 213.
43. A.M. Poskanzer, F.C. Goodrich, J. Phys. Chem. 79 (1975) 2122.
44. W.A. Gifford, L.E. Scriven, Chem. Eng. Sci. 26 (1971) 287.
45. M.A. Fortes, Can. J. Chem. 60 (1982) 2889.
46. C. Allain, M Cloitre, J. Colloid Interface Sci. 157 (1993) 261.
47. C. Allain, M Cloitre, J. Colloid Interface Sci. 157 (1993) 269.

For new developments on capillary forces between floating particles see also:

1. P.A. Kralchevsky, N.D. Denkov, Capillary forces and structuring in layers of colloid particles. Curr. Opin. Colloid Interf. Sci. 6 (2001) 383–401.
2. M.G. Nikolaides, A.R. Bausch, M.F. Hsu, A.D. Dinsmore, M.P. Brenner, C. Gay, D.A. Weitz, Electric-field-induced capillary attraction between like-charged particles at liquid interfaces. Nature 420, 299–301 (2002).
3. K.D. Danov, P.A. Kralchevsky, M.P. Boneva, Electrodipping force acting on solid particles at a fluid interface", Langmuir 20 (2004) 6139-6151.